Fc-engineered antibodies promote neutrophil-dependent control of *Mycobacterium tuberculosis*

Edward B. Irvine[1,2], Angel Nikolov[1,2], Mehak Z. Khan[1], Joshua M. Peters[1,3], Richard Lu[1], Jaimie Sixsmith[2], Aaron Wallace[4], Esther van Woudenbergh[1], Sally Shin[1], Wiktor Karpinski[1], Jeff C. Hsiao[1,3], Arturo Casadevall[5], Bryan D. Bryson[1,3], Lisa Cavacini[4], Patricia S. Grace[1,2], Galit Alter[1,6,7] ✉ & Sarah M. Fortune[1,2,7] ✉

Mounting evidence indicates that antibodies can contribute towards control of tuberculosis (TB). However, the underlying mechanisms of humoral immune protection and whether antibodies can be exploited in therapeutic strategies to combat TB are relatively understudied. Here we engineered the receptor-binding Fc (fragment crystallizable) region of an antibody recognizing the *Mycobacterium tuberculosis* (*Mtb*) capsule, to define antibody Fc-mediated mechanism(s) of *Mtb* restriction. We generated 52 Fc variants that either promote or inhibit specific antibody effector functions, rationally building antibodies with enhanced capacity to promote *Mtb* restriction in a human whole-blood model of infection. While there is likely no singular Fc profile that universally drives control of *Mtb*, here we found that several Fc-engineered antibodies drove *Mtb* restriction in a neutrophil-dependent manner. Single-cell RNA sequencing analysis showed that a restrictive Fc-engineered antibody promoted neutrophil survival and expression of cell-intrinsic antimicrobial programs. These data show the potential of Fc-engineered antibodies as therapeutics able to harness the protective functions of neutrophils to promote control of TB.

Mycobacterium tuberculosis (*Mtb*), the causative agent of tuberculosis (TB), remains the leading cause of death from a single bacterial infection globally, causing an estimated 1.3 million deaths in 2022 (ref. 1). As a result, novel therapeutic and vaccination strategies are urgently needed to slow the TB epidemic. To date, the majority of efforts to manipulate the immune response to drive control of TB have focused on potentiating cell-mediated immunity, as CD4 T cells play a critical role in controlling TB[2–4]. Little work has focused on harnessing the diverse effector mechanisms of humoral immunity to combat TB.

A growing body of evidence supports a functional role for antibodies in TB control. Importantly, mice lacking B cells, the cellular source of antibodies, exhibit enhanced susceptibility to *Mtb* disease[5]. Moreover, monoclonal and polyclonal antibody passive transfer studies have shown that antibodies alone can limit TB disease and spread[6–13]. It is noteworthy that antibodies binding surface-exposed

[1]Ragon Institute of MGH, MIT and Harvard, Cambridge, MA, USA. [2]Department of Immunology and Infectious Diseases, Harvard T. H. Chan School of Public Health, Boston, MA, USA. [3]Department of Biological Engineering, Massachusetts Institute of Technology, Cambridge, MA, USA. [4]MassBiologics of the University of Massachusetts Chan Medical School, Boston, MA, USA. [5]Department of Molecular Microbiology and Immunology, Johns Hopkins Bloomberg School of Public Health, Baltimore, MD, USA. [6]Division of Infectious Disease, Massachusetts General Hospital, Boston, MA, USA. [7]These authors contributed equally: Galit Alter, Sarah M. Fortune. ✉e-mail: galit.alter@modernatx.com; sfortune@hsph.harvard.edu
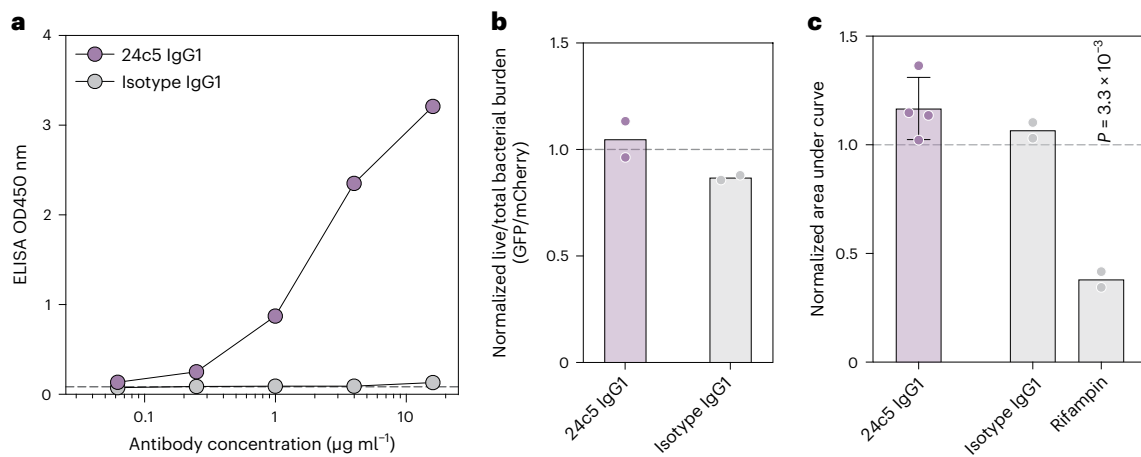
Fig. 1 | Wild-type IgG1 α-glucan antibody does not drive *Mtb* restriction in vitro. a, Glucan (bovine liver glycogen) antigen-binding ELISA of the α-glucan-specific antibody clone, 24c5. ELISA was run in technical duplicate. OD$_{450\,nm}$, optical density at 450 nm. **b**, Macrophage *Mtb* restriction assay. The *y* axis shows live (GFP)/total (mCherry) *Mtb* burden in human MDMs normalized by the no-antibody condition for the respective donor. Each point is the triplicate average from one human macrophage donor. **c**, Whole-blood *Mtb* restriction assay.

The *y* axis is the area under the *Mtb-276* growth curve value normalized by the no-antibody condition from the respective donor. Each point represents a triplicate average from one donor. One-way ANOVA with Dunnett's correction comparing each antibody or antibiotic with the isotype IgG1 control antibody. Adjusted *P* < 0.05 indicated. Error bar shows mean with standard deviation. Horizontal dashed lines indicate the no-antibody condition.

Mtb antigens have shown particular promise, displaying both an ability to reduce *Mtb* bacterial burden and to prolong survival in treated animals[6,7,12,14,15]. More specifically, several studies have found that antibodies specific to capsular polysaccharides, the outermost portion of the bacteria, promote *Mtb* uptake and significant *Mtb* control in vitro and in vivo[6,7,12,14,15]. These data highlight the potential for exploiting antibodies that recognize abundant surface-exposed *Mtb* glycans to prevent TB disease.

While it is plausible that simple antibody blockade of surface-exposed antigens represents a mechanism of antibody action against *Mtb*, antibodies may also prompt bacterial clearance following surface opsonization via Fc (fragment crystallizable) receptor engagement on local immune cells, allowing the activation of a diverse array of antimicrobial functions. Consistent with this model, antibody signalling via Fcγ receptors is required for optimal *Mtb* control in vivo[16], strongly implicating the immunoglobulin G (IgG) Fc in protective immunity against TB. Moreover, antibody Fc functional profiles differ across individuals who control *Mtb* infection and those with active, uncontrolled infection[17]. However, the primary mechanism(s) exploited by the antibody Fc to promote *Mtb* control have not been thoroughly assessed.

In this Article, we sought to develop a more detailed understanding of the effector mechanism(s) capsule-binding antibodies leverage to restrict *Mtb*. Thus, we rationally engineered a library of antibody Fc variants specific to α-glucan, an abundant, surface-exposed polysaccharide present in the *Mtb* capsule[18]. Each Fc variant was designed to augment or dampen select antibody effector functions based on data from the monoclonal therapeutics field (Supplementary Table 1). We demonstrate that IgG Fc engineering can significantly enhance the ability of α-glucan-specific antibodies to drive *Mtb* restriction in vitro. Fc-engineered α-glucan antibodies promoted *Mtb* restriction in a neutrophil-dependent manner, raising the possibility of exploiting Fc-engineered antibodies as a class of therapeutics able to use the antimicrobial activity of the innate immune system to drive TB control.

Results

Wild-type IgG1 α-glucan antibody does not restrict *Mtb*

The capsule, the outermost layer of *Mtb*, primarily comprises glucan and arabinomannan, which represent approximately 80% and 20% of the capsular polysaccharides, respectively[19,20]. While previous studies have shown that glucan elicits detectable antibody responses in mice and in humans[21–23], it remains unclear whether antibodies to this highly abundant antigen possess antimicrobial activity. Thus, to begin to probe the antimicrobial function of α-glucan-specific humoral immunity, we exploited a monoclonal antibody, clone 24c5, previously shown to bind *Mtb*[21].

Initially, the α-glucan-specific monoclonal antibody, 24c5, was generated as a human IgG1 monoclonal. Antigen binding to α-glucan was confirmed by enzyme-linked immunosorbent assay (ELISA) and compared to that of an isotype control antibody (Fig. 1a). Next, we sought to determine whether the α-glucan-specific IgG1 antibody was able to drive *Mtb* restriction in vitro. Human monocyte-derived macrophages (MDMs) were infected with a live/dead reporter strain of *Mtb* (*Mtb-live/dead*)[24], followed by the addition of antibody to the *Mtb*-infected cells. After 96 h, equivalent levels of intracellular *Mtb* restriction was observed in wells containing the α-glucan-specific IgG1 antibody and the isotype control (Fig. 1b). This assay interrogates the ability of antibodies to restrict bacterial growth solely in the presence of a previously infected macrophage, so we next queried whether the antibody could restrict infection in human whole blood—a system that captures the impact of multiple immune cell types and antibody functions at the time of bacterial exposure. Antibodies were added to fresh whole blood from healthy human donors at the same time as an auto-luminescent *Mtb* reporter strain (*Mtb-276*)[25]. Luminescence readings were then taken every 24 h over the course of 5 days to examine differences in *Mtb* growth curves across the α-glucan-specific and isotype control antibody conditions. Again, the α-glucan-specific IgG1 antibody did not show any evidence of *Mtb* restriction (Fig. 1c). Together, these data suggest that the α-glucan-specific IgG1 antibody did not mediate *Mtb* control in vitro.

Fc-engineered antibodies show diverse functional activity

Point mutations introduced into the antibody Fc domain at hotspots of Fc receptor and complement protein binding enable detailed analysis of the relationship between specific Fc-mediated functions and microbial control. Thus, to investigate the impact of antibody Fc profile on the restrictive capacity of *Mtb*-specific antibodies, we developed a library of 52 Fc-engineered IgG antibody variants with identical antigen-binding fragments (Fabs) as the original 24c5 antibody

clone using a high-throughput golden gate cloning approach (Supplementary Table 1)[26]. Fc variants included Fc modifications known to modulate specific antibody functions such as antibody-dependent cellular cytotoxicity (ADCC), antibody-dependent cellular phagocytosis (ADCP), antibody-dependent complement deposition (ADCD), and serum half-life extension (Supplementary Table 1)[26]. The 52 Fc variants of 24c5 were produced and tested for their ability to bind to α-glucan by ELISA. Each Fc-engineered antibody maintained binding comparable with that of the wild-type IgG1 antibody (Extended Data Fig. 1a), indicating that antibody Fc modifications did not impede α-glucan binding activity. Furthermore, glycosylation analysis revealed that Fc glycans were largely dominated by structures lacking galactose (Extended Data Fig. 1b).

We next characterized the differential impact of each 24c5 variant on Fc-effector functions. We used α-glucan or α-glucan-containing *Mtb* whole-cell lysate rather than live bacteria to enable the high-throughput functional profiling of each Fc variant. Specifically, we probed the ability of each Fc-engineered antibody to drive natural killer (NK) cell activation (antibody-dependent NK cell activation (ADNKA)), complement deposition (ADCD), monocyte phagocytosis (ADCP) and neutrophil phagocytosis (antibody-dependent neutrophil phagocytosis (ADNP)) (Fig. 2 and Extended Data Fig. 1c). As expected, in the ADNKA assay, a surrogate for ADCC, Fc variants engineered to have potent ADCC activity, such as SDIEALGA[27], SAEAKA[28] and I332E (Supplementary Table 1)[29], elicited increased NK cell degranulation (CD107a) and NK cell activation (interferon-γ (IFNγ) and MIP-1β secretion) compared with the wild-type IgG1 antibody (Fig. 2 and Extended Data Fig. 1c). 24c5 Fc variants, such as KWES[30], K326W[30] and HFST[31], designed to have increased complement activity (Supplementary Table 1), mediated increased complement component 3b (C3b) deposition compared with the wild-type IgG1 antibody (Fig. 2 and Extended Data Fig. 1c). Similarly, 24c5 Fc variants engineered to facilitate enhanced monocyte phagocytosis, such as SDIEGA[32], SDIEAL[29] and SDIE[29] (Supplementary Table 1), mediated increased monocytic uptake of *Mtb* whole-cell lysate-coated beads compared with the wild-type IgG1 antibody (Fig. 2 and Extended Data Fig. 1c). Further, while the ability of these Fc variants to mediate neutrophil phagocytosis has not been as thoroughly assessed, several Fc-engineered α-glucan antibodies, such as SEHFST LS[26,31], SDIESA LS[26,33] and IgG3 RH[34], drove robust neutrophil phagocytosis of *Mtb* whole-cell lysate-coated beads compared with the wild-type IgG1 antibody (Fig. 2 and Extended Data Fig. 1c). From a combinatorial perspective, Fc variants emerged with different combinations of antibody effector profiles (Fig. 2 and Extended Data Fig. 1c). Yet, the N297Q variant, a non-glycosylated Fc variant designed to have minimal affinity for Fcγ receptors[35,36], showed limited activity across the functional profiling assays as expected (Fig. 2 and Extended Data Fig. 1c).

Half-life extending mutations (M428L/N434S; LS) were added to numerous Fc variants in the panel[37]. Comparing the 'normal' and 'LS' half-life extended versions showed significant correlations across the ADNKA (MIP-1β) and ADNKA (IFNγ) assays (Extended Data Fig. 1d) and moderate, yet insignificant, correlations across the ADCD and ADCP assays (Extended Data Fig. 1d). This indicates that the functional profiles of the paired variants was similar but not identical. Furthermore, a similar Fc-variant panel was profiled in a previous study using the Ebola glycoprotein-specific monoclonal antibody, VIC16 (ref. 26). Correlating functional results across the 24c5 and VIC16 panels revealed significant positive correlations in the ADNKA (CD107a), ADNKA (MIP-1β), ADNKA (IFNγ) and ADCD assays but not in the phagocytosis assays (ADCP and ADNP) (Extended Data Fig. 1e). The inconsistency of antibody-mediated monocyte and neutrophil phagocytic responses may be explained by pathogen-associated molecular patterns present in *Mtb* whole-cell lysate that may engage pathogen recognition receptors and activate these cells. Collectively, these data indicate that Fc engineering shifts the functional profile of α-glucan-specific antibodies, driving variable enhancement or diminution of several effector functions and providing a wide array of combinatorial functional responses to interrogate Fc-mediated restriction of *Mtb*.

Fc-engineered antibodies down-selected by functional profile

To test the antimicrobial properties of α-glucan-specific antibodies with different Fc-effector profiles, we sought to reduce the number of α-glucan Fc variants while maintaining the functional heterogeneity present in the full monoclonal library. To this end, the α-glucan Fc variants were hierarchically clustered using all the functional profiling data. At least one variant was selected from each of the 11 clusters that emerged (Fig. 3a), capturing the diversity in antibody functional profiles across the Fc-variant library. The ultimate down-selected 24c5 panel included Fc variants with several types of functional activity (Fig. 3b). For instance, the down-selected panel included M252Y/S254T/T256E (YTE) (which solely possessed monocyte phagocytic function)[38], IgG3 RH (which showed robust complement and phagocytic functions)[34], I332E (which had potent NK activating properties)[29] and N297Q (a largely non-functional and non-glycosylated Fc variant) (Fig. 3b)[35,36]. Thus, while the down-selected α-glucan Fc-variant panel comprises fewer variants, substantial heterogeneity was maintained, providing a robust starting point from which to define the relationship between antibody functional profiles and *Mtb* restriction.

Select Fc-engineered antibodies restrict *Mtb* in whole blood

While the wild-type 24c5 IgG1 antibody did not significantly restrict *Mtb* (Fig. 1), we next aimed to determine whether the addition of certain Fc functions to the 24c5 antibody clone could augment bacterial restriction in vitro. Fresh whole blood from healthy human donors was simultaneously infected with *Mtb-276* (ref. 25) and treated with each 24c5 antibody. While the wild-type IgG1 antibody did not mediate significant *Mtb* restriction, 6 of the 15 down-selected Fc-engineered antibodies tested drove significant *Mtb* restriction in whole blood compared with the IgG1 isotype control antibody (Fig. 4a). No significant correlation was observed between restriction activity in whole blood and α-glucan antigen binding, indicating that the restrictive effect was not simply due to subtle differences in antigen binding between the variants (Fig. 4b). Conversely, none of the Fc variants tested drove intracellular *Mtb* killing in macrophages alone (Extended Data Fig. 2), suggesting the mechanistic involvement of additional immune effectors present in peripheral blood in antibody-mediated restriction in vitro.

To explore the immune milieu driven by restrictive antibody treatment, we profiled cytokine levels 120 h following *Mtb* infection and antibody treatment in whole blood across multiple donors (Fig. 4c,d and Extended Data Fig. 3a–d). Restrictive Fc variants elicited a distinct cytokine profile, marked by a selective enrichment in secreted IFNγ and interleukin-10 (IL-10) compared with Fc variants that were non-restrictive (Fig. 4c,d and Extended Data Fig. 3a–d). These cytokine differences were significant at a univariate level (Extended Data Fig. 3a,d). While there was heterogeneity in the secretion of additional cytokines including IL-6, IL-8 and IL-1β, these cytokines did not distinguish restrictive versus non-restrictive α-glucan antibody Fc variants (Fig. 4c,d and Extended Data Fig. 3a–d). To determine whether the restrictive effect promoted by the Fc-optimized 24c5 SEHFST LS variant was dependent on particular cytokines, we performed cytokine blockade experiments in the whole-blood assay. IFNγ blockade resulted in a significant loss in *Mtb* control independent of 24c5 antibody treatment (Extended Data Fig. 3e), while IL-1β blockade did not significantly alter *Mtb* control in an antibody-dependent manner (Extended Data Fig. 3e). Together, these data indicate that Fc variants can restrict *Mtb*, and they highlight distinct cytokine/inflammatory responses associated with restrictive antibody treatment.

Fc variants drive neutrophil-dependent *Mtb* restriction

To probe the mechanism(s) exploited by Fc variants to restrict *Mtb* growth in whole blood, we next assessed the relationship between
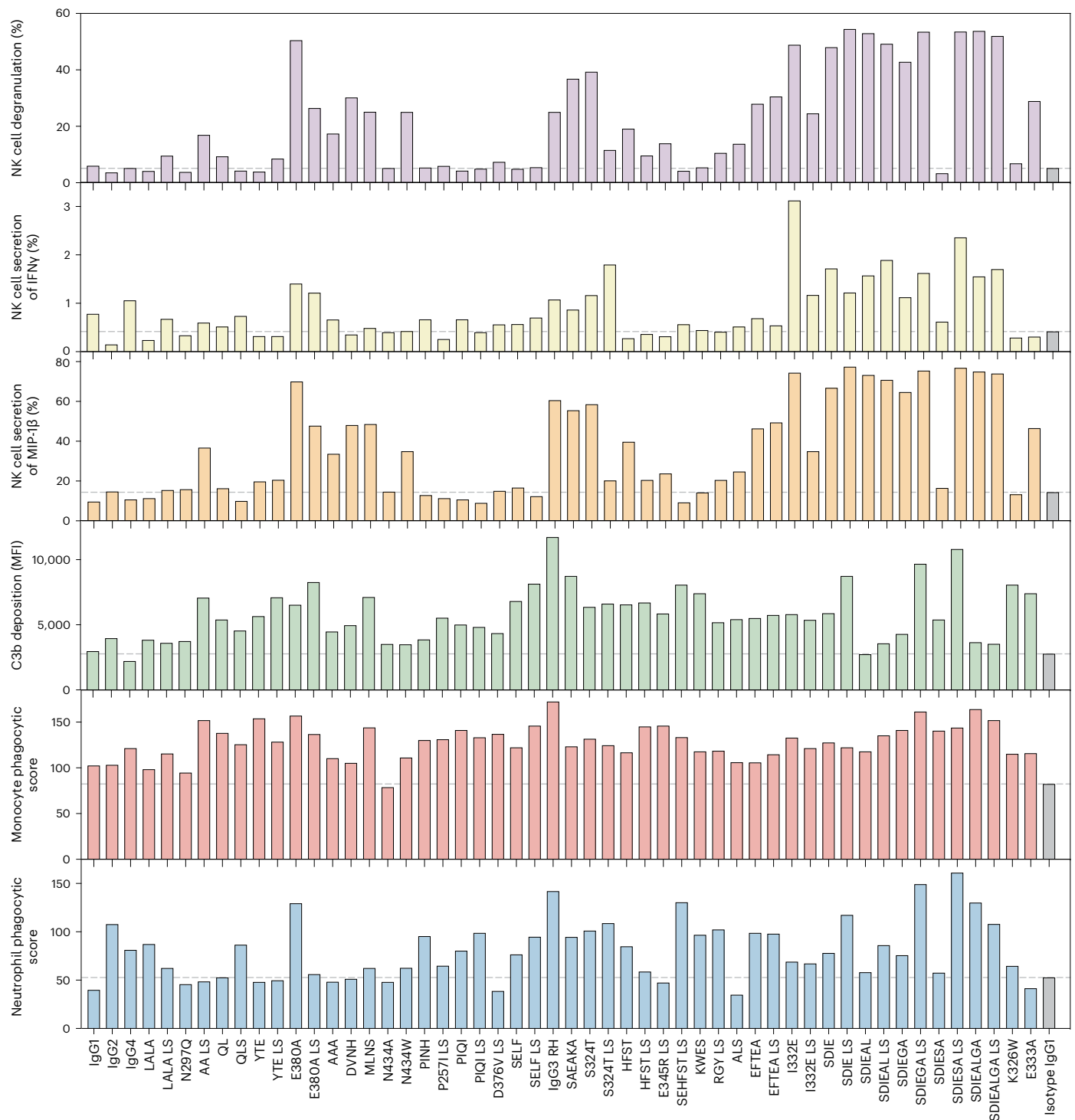
Fig. 2 | Fc-engineered α-glucan antibodies show a range in functional activity. The ability of each α-glucan Fc variant to mediate (from top to bottom) NK cell degranulation (ADNKA), NK cell secretion of IFNγ (ADNKA), NK cell secretion of MIP-1β (ADNKA), complement component 3b (C3b) deposition (ADCD), phagocytosis by THP-1 monocytes (ADCP) and phagocytosis by primary human neutrophils (ADNP) was experimentally determined. Each antibody was run in duplicate across each assay, and the mean functionality is shown. Grey dashed line indicates the performance of an IgG1 isotype control antibody. See Methods for the experimental details of each assay.

the whole-blood restriction assay (WBA) and each of the functional profiling assays (Fig. 5a). ADNP showed a significant negative correlation with *Mtb* growth in whole blood (Fig. 5a). We had anticipated that antibodies able to drive potent functions across multiple immune effectors would optimally restrict *Mtb*, yet, unexpectedly, antibodies which were not broadly functional, and instead selectively induced neutrophil phagocytosis, significantly restricted growth in whole blood (Fig. 5b). While purified-protein-derivative-specific IgG with increased FcγR3A binding and NK cell activating activity was previously associated with control of *Mtb* in macrophages[17], we found that antibody-dependent NK cell degranulation (CD107a) and activation (IFNγ and MIP-1β secretion) activity of monoclonal α-glucan Fc variants positively correlated with *Mtb* growth in whole blood (Fig. 5a). This divergence in protective Fc profile suggests that antibodies targeting
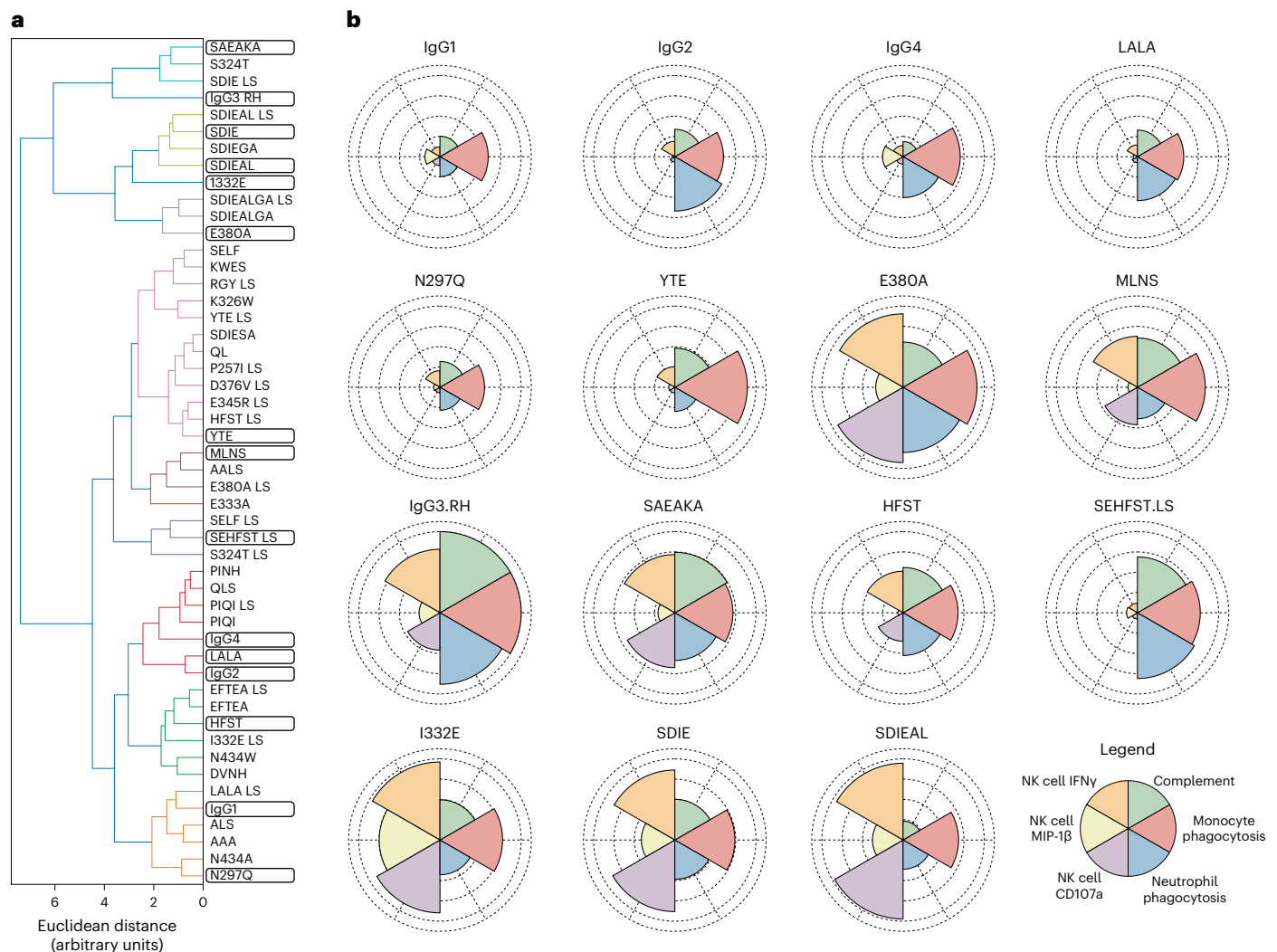
Fig. 3 | Hierarchical clustering used for the rational down-selection of Fc-engineered α-glucan antibodies. a, Cluster dendrogram of the α-glucan Fc-variant panel following complete-linkage hierarchical clustering of the functional profiling data. At least one variant from each cluster (boxed) was selected for antimicrobial profiling. **b**, Polar plots highlighting the functional profile of each α-glucan Fc variant in the down-selected panel. Each pie piece indicates the magnitude of functionality in the respective assay relative to the entire panel. The α-glucan Fc variants were max-scaled before polar plot visualization.

different antigens may leverage distinct immune effector mechanisms to promote *Mtb* control.

To test the hypothesis that the engagement of neutrophils by restrictive Fc-engineered α-glucan antibody variants was key to *Mtb* restriction in the whole-blood model of infection, neutrophils were depleted from blood before infection and the addition of select Fc-engineered antibodies. The SEHFST LS and SAEAKA α-glucan Fc variants previously found to drive *Mtb* restriction no longer restricted *Mtb* in the absence of neutrophils (Fig. 5c). These Fc variants maintained their restrictive activity when monocytes were depleted instead of neutrophils (Extended Data Fig. 4a) and when complement was inhibited using cobra venom factor (Extended Data Fig. 4b)[39], although cobra venom factor led to a reduction of *Mtb* luminescence even in the absence of restrictive antibody treatment (Extended Data Fig. 4b). In addition to the synthetic SEHFST LS and SAEAKA Fc variants, the IgG2 and IgG4 naturally occurring Fc variants showed significantly less restrictive activity in the absence of neutrophils (Fig. 5c). As expected, neither the wild-type IgG1 nor the N297Q antibody variants drove *Mtb* restriction irrespective of immune cell depletion (Fig. 5c and Extended Data Fig. 4a). Collectively, these data indicate that several Fc-modified α-glucan antibodies leverage neutrophil function to drive *Mtb* control.

SEHFST LS variant upregulates neutrophil antimicrobial genes

Neutrophils have been associated with both protection and pathology in *Mtb* infection[40]. Several studies have described neutrophils as an early microbial reservoir in naive hosts, controlling intracellular *Mtb* less effectively compared with macrophages[41,42], and over the course of infection, neutrophil recruitment is associated with necrosis and caseation[40,43]. However, in other environments neutrophils have been found to have potent ability to clear *Mtb*, activity that is suppressed by granulocyte necrosis[44]. The observation that select Fc-engineered antibodies promoted *Mtb* restriction in a neutrophil-dependent manner suggested that the presence of Fc-optimized antibodies at the time of bacterial exposure may trigger molecular circuits in neutrophils that direct neutrophil antimicrobial functions. Hence, we next performed single-cell RNA sequencing (scRNA-seq) to characterize the effects of Fc-optimized antibody treatment. Fresh whole blood from three healthy human donors was infected with *Mtb* and treated with either the 24c5 IgG1 or the Fc-optimized 24c5 SEHFST LS antibody variant. Conditions without monoclonal antibody (no Ab) and without *Mtb* (uninfected) were additionally included as controls. We performed scRNA-seq analysis of the whole-blood cell populations under the
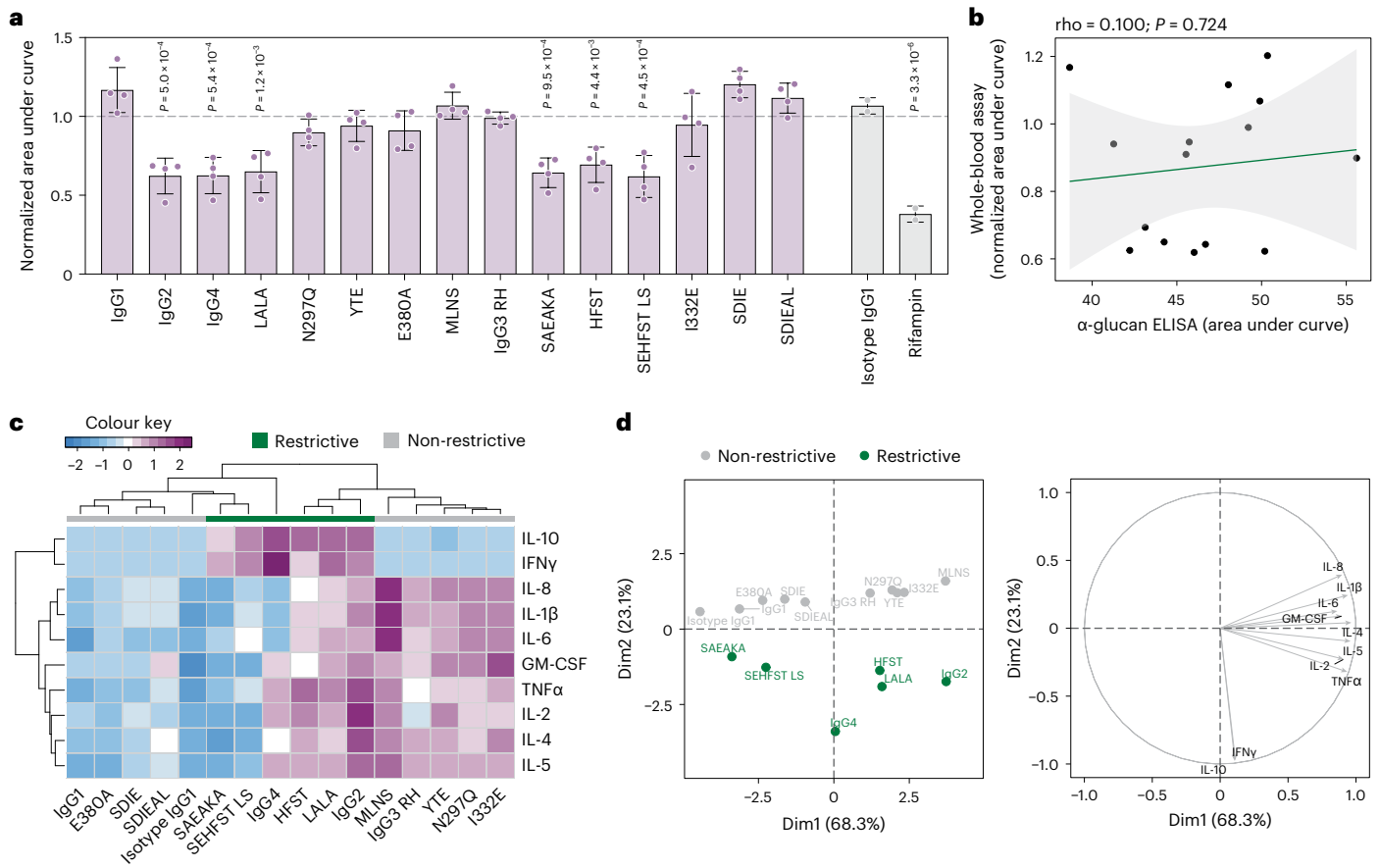
Fig. 4 | Several Fc-engineered α-glucan antibodies drive *Mtb* restriction in whole blood. a, Whole-blood *Mtb* restriction assay. The *x* axis shows the different α-glucan Fc variants (25 μg ml⁻¹), an IgG1 isotype control antibody as a negative control (25 μg ml⁻¹) and the antibiotic rifampin as a positive control (0.25 μg ml⁻¹). The *y* axis is the area under the *Mtb-276* growth curve value normalized by the no-antibody condition from the respective donor. Each point represents a triplicate average from one donor. One-way ANOVA with Dunnett's correction comparing each antibody or antibiotic with the isotype IgG1 control antibody. Adjusted *P* < 0.05 are indicated. Error bars show mean with standard deviation. Horizontal dashed line indicates the no-antibody condition. **b**, Spearman

correlation between the normalized area under the curve in the whole-blood assay and α-glucan antigen binding determined via ELISA. Spearman correlation was two-sided. Green solid line is the linear regression line; grey shading indicates the 95% confidence interval. **c,d**, Cytokine Luminex using the whole-blood assay supernatant collected at 120 h. Triplicate average from donor A shown. **c**, Clustered heat map indicating the cytokine profile elicited by each α-glucan Fc variant. Data were *z*-scored before heat map visualization. **d**, PCA of cytokine Luminex data. Left: score plot of the first two principal components. Right: loading plot of the first two principal components. The *x* and *y* axes are principal components 1 and 2, respectively.

various conditions at 24 h to maximize neutrophil recovery and to capture early Fc-mediated signals within cells of whole blood.

Cells were clustered into 1 of 21 different cell subsets by their gene expression and visualized in low dimensional space through uniform manifold approximation and projection (UMAP) (Fig. 6a). Following quality control, 7,334 total cells and 906 neutrophils were recovered. The 24c5 SEHFST LS variant showed an increased proportional abundance of neutrophils compared with the other treatment conditions (Fig. 6b). These data suggest increased survival of neutrophils in the presence of the Fc-optimized antibody compared with the control conditions.

Consistent with this, expression of *PI3*, which encodes trappin-2, an inhibitor of neutrophil elastase that may be associated with prevention of Netosis and alternative antimicrobial functions[45,46], was increased in the 24c5 SEHFST LS condition compared with the 24c5 IgG1 and no Ab conditions (Fig. 6c). Expression of *FTH1*, which encodes a subunit of ferritin, the major intracellular iron storage protein in eukaryotes[47], was also higher in the setting of 24c5 SEHFST LS antibody treatment (Fig. 6c), suggesting that the Fc-optimized antibody may modulate intracellular iron availability for the bacterium. Conversely, gene expression of *BASP1* (brain abundant signal protein 1), which is associated with cell death and senescence[48–50], was decreased following 24c5 SEHFST LS antibody treatment (Fig. 6c).

Gene Ontology (GO) analysis of the differentially expressed genes following 24c5 SEHFST LS antibody treatment (Fig. 6d) found key antimicrobial circuits leveraged by neutrophils to drive control of intracellular pathogens including neutrophil degranulation[51,52], sequestration of iron[53] and the response to IFNγ, to be significantly upregulated following 24c5 SEHFST LS treatment (Fig. 6d). By contrast, analysis of the differentially expressed genes in the CD14⁺ monocytes from the 10X dataset revealed downregulation of the gene encoding toll-like receptor 2 (*TLR2*) and the GO biological processes involved in the response to cytokines following 24c5 SEHFST LS antibody treatment (Extended Data Fig. 5). Taken together, these data suggest that 24c5 SEHFST LS may divert the antimicrobial recognition and response to *Mtb* from the CD14⁺ monocyte to the neutrophil compartment, promoting neutrophil survival and the selective and sustained upregulation of antimicrobial gene programs that may contribute to intracellular *Mtb* control.

Discussion

Here we used an Fc-engineering approach to (1) determine whether rational Fc modification could enhance antibody restrictive capacity and (2) define the innate immune mechanism(s) that antibodies may leverage to restrict *Mtb*. We demonstrated that IgG Fc engineering
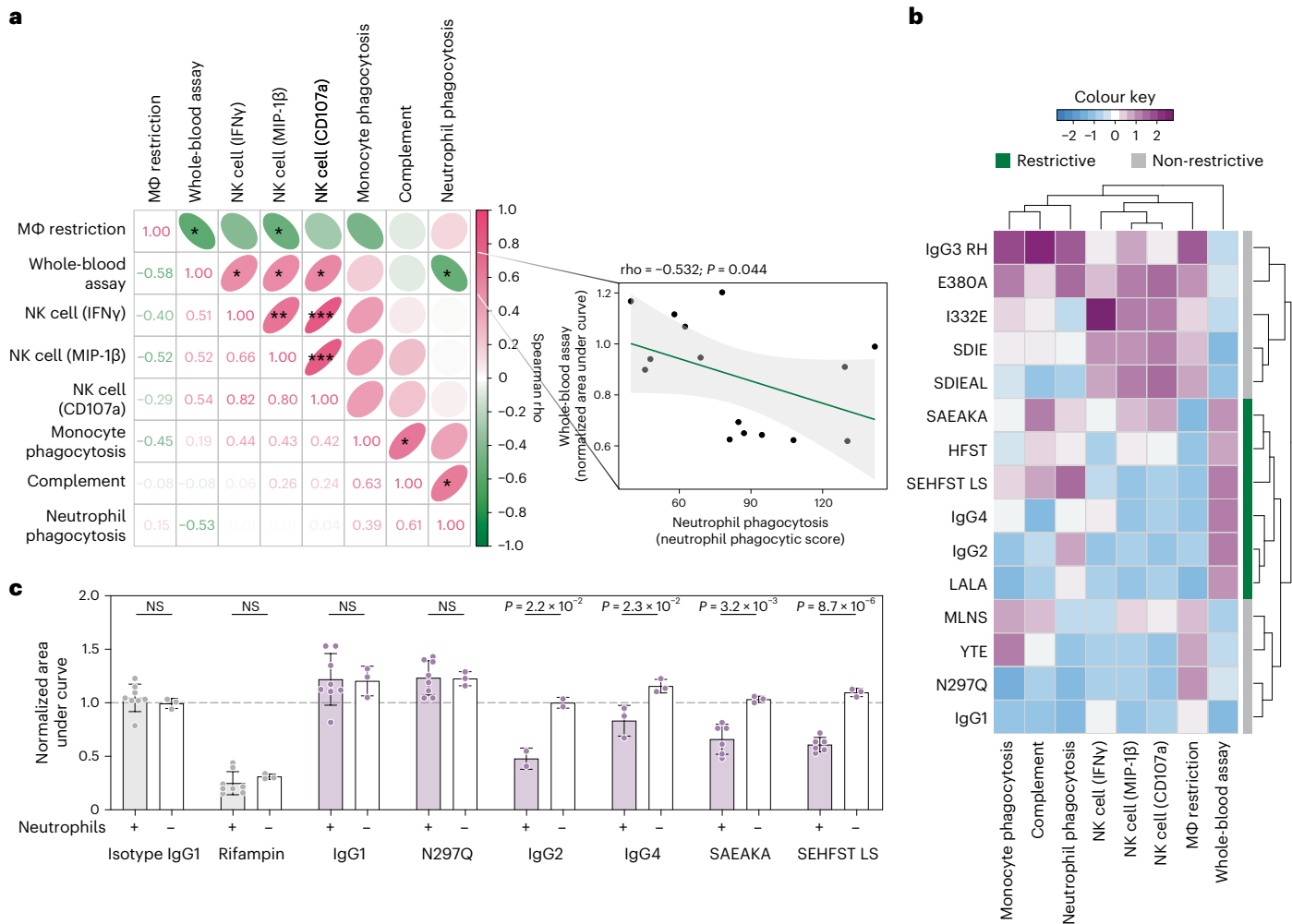
Fig. 5 | Fc-engineered α-glucan antibodies drive *Mtb* restriction in a neutrophil-dependent manner. a, Spearman correlation matrix of the different functional and antimicrobial assays. The bottom left section of the correlation matrix indicates the Spearman correlation coefficient for each relationship. The upper right section of the correlation matrix contains ellipses that have their eccentricity parametrically scaled to the strength of the correlation for each relationship. Pairwise correlation between the normalized area under the curve in the whole-blood assay and the phagocytic score from the neutrophil phagocytosis assay is highlighted. Grey-shaded error band shows 95% confidence interval. Spearman correlations were two-sided. *P < 0.05; **P < 0.01; ***P < 0.001. **b**, Clustered heat map indicating the performance of each α-glucan Fc variant in the down-selected panel across different functional and antimicrobial assays. Data were z-scored before heat map visualization. **c**, Whole-blood *Mtb* restriction

assay with neutrophil depletions. The *x* axis shows selected α-glucan Fc variants (25 μg ml^{-1}), an IgG1 isotype control antibody as a negative control (25 μg ml^{-1}) and the antibiotic rifampin as a positive control (0.25 μg ml^{-1}). Each antibody or antibiotic treatment was tested in whole blood (filled-in bars) and neutrophil-depleted blood (white bars). The *y* axis is the area under the *Mtb-276* growth curve value normalized by the no-antibody condition from the respective donor. Each point represents a triplicate average from one donor. Two-tailed, unpaired *t*-test, comparing restriction in the neutrophil-depleted blood condition with the whole-blood condition for each treatment. Error bars show mean with standard deviation. Unadjusted *P* < 0.05 are indicated, and comparisons labelled as 'NS' (not significant) have unadjusted *P* > 0.05. Horizontal dashed line indicates the no-antibody condition.

can significantly augment the ability of α-glucan antibodies to drive *Mtb* restriction in vitro, pointing to a unique strategy for the development of therapeutics to combat TB. Unexpectedly, several Fc-engineered α-glucan antibodies drove *Mtb* restriction in a neutrophil-dependent manner. These data further suggest that antibodies can harness the antimicrobial potential of neutrophils to promote *Mtb* restriction by selectively rewiring neutrophils at the transcriptional level.

We demonstrate that a subset of Fc optimized IgG antibodies specific to the *Mtb* capsule mediate improved bacterial restriction over the wild-type IgG1 antibody in a whole-blood model of infection. This finding contributes to a growing body of evidence pointing to the biophysical characteristics of the antibody Fc as a critical determinant of antibody protective activity in the context of *Mtb* infection[10,13,17,54,55]. Indeed, antibody signalling through Fcγ receptors is required for optimal *Mtb* control in mice[16]. More recently, Fcγ receptor engagement was

shown to be necessary for the protective function of several monoclonal antibodies specific to the *Mtb* phosphate transporter subunit PstS1 (ref. 10). In addition, isotypes including IgA and IgM have shown enhanced antimicrobial function over IgG1 antibodies across various models of *Mtb* infection[13,54–56]. While the precise mechanisms of antibody Fc-mediated *Mtb* control have yet to be elucidated, this collection of work suggests that in many cases, simply altering the Fc region is sufficient to make antibodies better at the task of controlling *Mtb* growth. In this study, we had the opportunity to map Fc effector mechanisms of action for monoclonal antibody specific to a single antigenic target−α-glucan. For this particular clone, we found that antibodies promoted *Mtb* control in a neutrophil-dependent manner. Yet importantly, Fc effector functions which promote *Mtb* control in the context of this capsule-specific antibody may not represent a generalizable protective Fc profile in the context of *Mtb*-specific
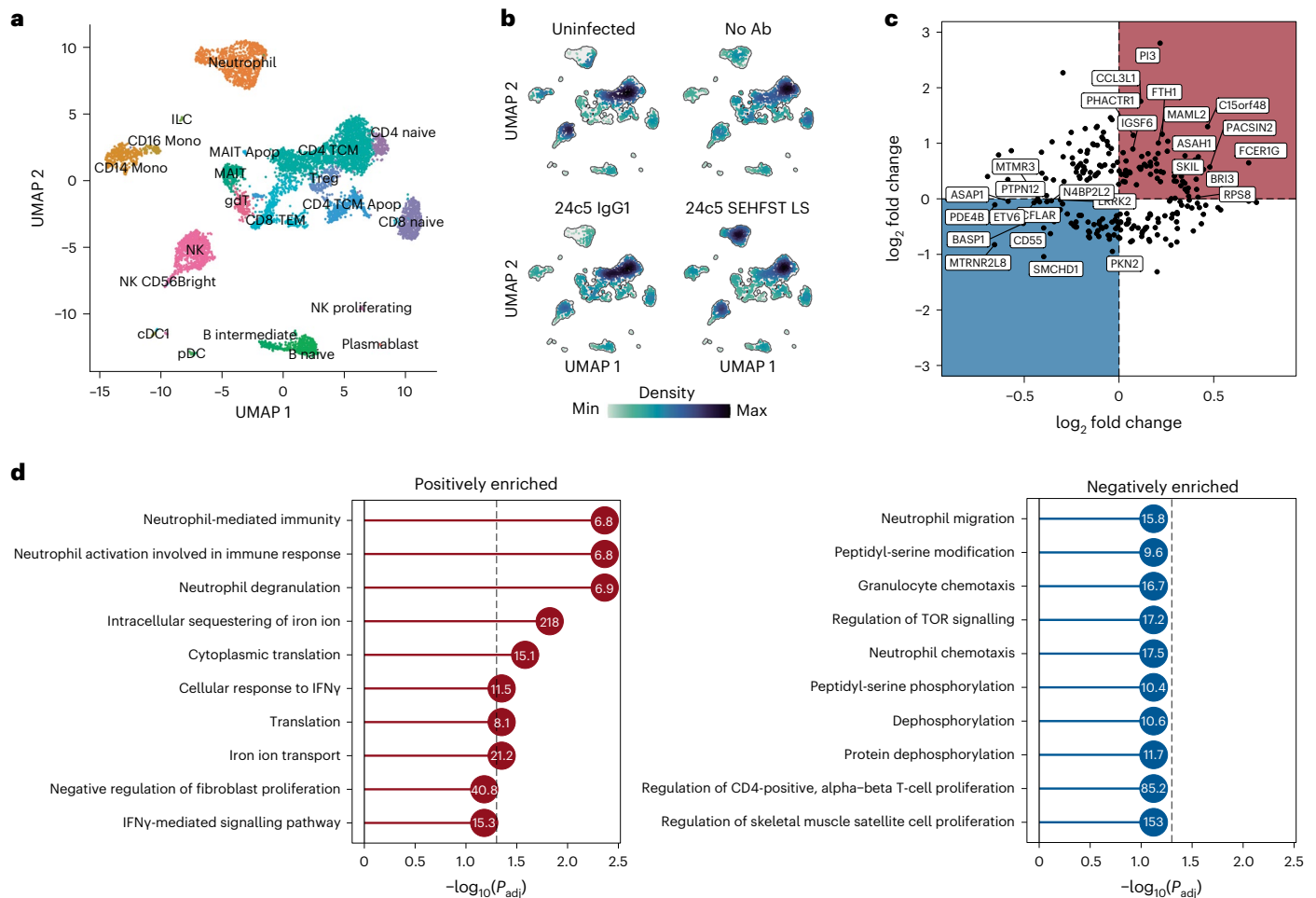
Fig. 6 | 24c5 SEHFST LS drives the upregulation of antimicrobial gene programs in neutrophils. a, Uniform manifold approximation and projection (UMAP) visualization of all cells and cell subsets recovered following scRNA-seq. The *x* and *y* axes represent the first and second dimensions of the UMAP embedding respectively. **b**, UMAP depicting fractional abundance (density) in different cell types across treatment groups. **c**, Neutrophil differential expression analysis. The *x* and *y* axes indicate $\log_2$ fold change of the SEHFST LS variant compared with the no antibody and the IgG1 conditions, respectively. Genes consistently increased in the 24c5 SEHFST LS condition (red quadrant): (1) Mann–Whitney $P < 0.1$ and a $\log_2$ fold change > 0.25 compared with either the 24c5 IgG1 or no Ab condition, (2) detected in a minimum fraction of 0.1 cells in either of the two conditions and (3) a $\log_2$ fold change > 0 compared with both

the 24c5 IgG1 and no Ab conditions. Genes consistently decreased in the 24c5 SEHFST LS condition (blue quadrant): (1) Mann–Whitney $P < 0.1$ and a $\log_2$ fold change < −0.25 compared with either the 24c5 IgG1 or no Ab conditions, (2) detected in a minimum fraction of 0.1 cells in either of the two conditions and (3) a $\log_2$ fold change < 0 compared with both the 24c5 IgG1 and no Ab conditions. Mann–Whitney tests were two-sided. **d**, Gene list enrichment analysis using GO Biological Process gene sets. The *x* axis indicates the adjusted *P* value of each GO term. Left: GO terms enriched in red quadrant genes from **c**. Right: GO terms enriched in blue quadrant genes from **c**. Vertical dashed line indicates two-sided Fisher's exact test adjusted *P* value of 0.05. Numbers on each circle show the odds ratio. Top ten GO terms by adjusted *P* value shown.

antibodies. The 24c5 antibody clone was originally generated via mouse immunization[21], and it remains unclear how the gain-of-function Fc mutations identified would be reflected in the functionality of antibodies arising from natural *Mtb* infection in humans. Moreover, antibodies targeting different antigens, or even epitopes, may leverage distinct immune effector mechanisms to drive protection against the bacteria. For instance, in previous work, ADCC via FcγR3A binding was found to be associated with improved polyclonal antibody-mediated *Mtb* control in a macrophage model of infection[17]. In the context of multiple PstS1-specific monoclonal antibodies, a combination of FcγR2A (CD32) and FcγR3A (CD16) binding was essential for antimicrobial function[10]. Hence, it is likely that no singular Fc profile universally drives control of *Mtb* and that antimicrobial function may instead be antigen- and context-dependent. Future studies aimed at mapping humoral immune mechanisms of action in the context of additional targets may provide further insights into the unique Fc-mediated mechanisms that may be leveraged across the landscape of *Mtb* antigens to control the pathogen.

The mechanism(s) of action of the Fc-optimized antibodies identified is not immediately obvious based on their previously published functionalities. Three of the restrictive variants represent low-effector variants (IgG2, IgG4 and L234A/L235A)[57], two were designed to have enhanced complement activity (HFST and SEHFST LS)[26,31], and one was designed to drive enhanced ADCC (SAEAKA)[28]. Yet our agnostic approach characterized by in-depth functional profiling of each variant suggested that antibodies able to deploy neutrophil function significantly restricted *Mtb* growth in whole blood, emphasizing the importance of characterizing antibodies across a range of functional assays during the development process.

Activation of neutrophils represents a delicate and context-dependent balancing act. The robust destructive and inflammatory functions of neutrophils have been associated with the development of more severe TB disease late in infection[58,59]. Given that poorly functional antibodies are abundant during active pulmonary *Mtb* infection[17,60], it is plausible that these antibodies may exacerbate suboptimal neutrophil

functions late in *Mtb* infection rather than ameliorate TB disease. However, upon initial *Mtb* exposure, neutrophils are first recruited into the airways and lung tissue at a time when adaptive immune responses are yet to develop and thus are in the presence of limited antigen-specific IgG antibodies. Conversely, in the present study, we observed that the pre-existence of *Mtb*-specific neutrophil-activating antibodies at the time of *Mtb* infection rewires neutrophils, promoting neutrophil survival and bacterial restriction. Our results show that the efficacy of neutrophils against mycobacteria is highly dependent on whether the interaction involves immunoglobulin opsonins and the type of engagement of Fc receptors. Consequently, vaccines that elicit antibodies that facilitate neutrophil activity against mycobacteria could protect by enhancing the efficacy of these innate immune response cells. In this respect, previous analysis of bronchoalveolar lavage fluid from non-human primates immunized with protective intravenous Bacillus Calmette–Guérin identified a significant expansion of antibodies able to arm neutrophil activity in the lung[56].

The combination of Fc engineering with single-cell transcriptomics pointed to unexpected Fc-mediated antibody therapeutic strategies as alternatives in the face of expanding antibiotic resistance. Specifically, transcriptomic analysis suggested a need for neutrophil survival and degranulation for optimal antibody-mediated *Mtb* restriction. While macrophages and monocytes shunt phagosomal contents into the endocytic maturation pathway, gradually converting the phagosome into a phagolysosome, neutrophils instead possess a myriad of preformed granules containing antimicrobial peptides and lytic enzymes that rapidly fuse with the phagosome following Fcγ-mediated uptake[52]. Thus, it is plausible that neutrophil survival, if long enough to permit the unique phagosome-targeted degranulation process downstream of Fcγ-mediated phagocytosis in neutrophils, may contribute to intracellular *Mtb* control. More complex multicellular functions may also contribute to control. Indeed, the significant increase in IL-10 release induced by restrictive Fc variants hints that Fc-optimized antibodies may promote a phenotypic switch in neutrophils to become high IL-10 producers that regulate *Mtb*-induced inflammation[61]. While neutrophils are the most abundant leukocyte in the blood, only around 12% of the cells interrogated during scRNA-seq analysis were neutrophils. This is not unexpected as neutrophils are particularly susceptible to apoptosis upon ex vivo manipulation. Furthermore, low RNA content and high levels of endonucleases in neutrophils typically result in a low number of quality sequencing reads even in settings of high neutrophil viability. Thus, while neutrophil numbers were sufficient in the present study to nominate several processes that may contribute to *Mtb* control, it is conceivable that protective neutrophil populations and/or functions may have been missed in the analysis due to technical limitations.

Invulnerable to antibiotic resistance, antibody-based therapeutics against TB represent an appealing modality. Thus, while little investigative effort has focused on harnessing humoral immunity to combat TB, our work shows the value of exploiting Fc engineering and single-cell transcriptional analysis to identify antibody-mediated mechanisms of *Mtb* control and to inspire next-generation antibody-based therapeutic design.

Methods

Ethics statement
This study was conducted in accordance with all relevant ethical regulations and guidelines. The study was approved by the institutional review board at Massachusetts General Hospital.

Fc engineering
A golden gate cloning strategy was used for antibody Fc engineering following established protocols[26,62]. In short, restriction sites for the type IIS restriction enzyme BsaI were inserted flanking the sequences of the different antibody domains, including variable heavy, variable light, and constant light domains, as well as the constant heavy domain (which was distinct for each Fc variant). Additionally, a furin 2A domain was inserted. BsaI generates a set of unique overhangs, allowing the antibody expressing plasmid to be generated in a single-step digestion/ligation reaction. The furin 2A site mediates self-cleavage of the polypeptide and thus expression of the entire antibody from a single open reading frame[63]. Each plasmid was sequenced to confirm the accuracy of golden gate assembly.

Antibody expression and purification
For antibody functional profiling and the whole-blood and macrophage restriction screens, antibody expressing plasmids were co-transfected with an additional antibody variable light plasmid at a 1:1 ratio into CHO cells. Although not strictly necessary for antibody expression, co-transfecting with the additional antibody variable light plasmid was found to boost expression levels. Antibody was purified from the cell supernatant using a Prosep-vA Ultra Protein A resin. Antibody was then dialysed and concentrated in phosphate-buffered saline (PBS). Concentration was determined by ELISA through comparison with a wild-type IgG1 antibody standard. For the blood depletion and scRNA-seq experiments, antibody expressing plasmids were co-transfected with an additional antibody variable light plasmid at a 1:1 ratio into 293F suspension cells following an established protocol[26]. Antibody was purified from the cell supernatant using Protein G magnetic beads (Millipore, LSKMAGG10) and concentrated in PBS. Concentration was determined by BCA protein assay through comparison with a bovine gamma globulin standard (Thermo Fisher, 23225). Biochemical quality was assessed by non-reducing gel and A280 measurements (Supplementary Fig. 1).

Glucan ELISA
ELISA plates (Thermo Fisher, NUNC MaxiSorp flat bottom) were coated with 50 µl of bovine liver glycogen (Milipore Sigma, G0885) at 100 µg ml^{-1} overnight at 4 °C. The plates were washed with PBS and blocked with 5% bovine serum albumin (BSA)–PBS for 2 h at room temperature on an orbital shaker. The plates were washed with PBS; then 80 µl of antibody was added in 4-fold dilutions ranging from 16 µg ml^{-1} to 0.0625 µg ml^{-1}, and the plate was incubated for 1.5 h at room temperature on an orbital shaker. Human IgG1 isotype control antibody was used as negative control (Immune Technology, IT-001-37G12). The plates were washed with PBS; then 80 µl of secondary anti-human Igκ light chain HRP-conjugated antibody (Thermo Fisher, A18853) diluted to 1:1,000 in 0.1% BSA–PBS was added. The plates were incubated for 1 h at room temperature on an orbital shaker. The plates were washed with PBS; then 80 µl per well of TMB (Thermo Fisher, 34029) was added. The reaction was stopped using 2 N H$_2$SO$_4$, and absorbance was measured at 450 nm on a plate reader (Tecan Infinite M1000 Pro).

Glycosylation analysis
Fc glycosylation analysis was performed following an established protocol[60]. In brief, 20 µg of each 24c5 Fc variant was digested with IdeS (Promega) at 37 °C for 1 h. Fc domains were selected using protein G beads (Millipore) at room temperature for 1 h. Glycans were isolated from Fc fragments and labelled using the Glycan Assure APTS kit according to the instructions of the manufacturer (Life Technologies, A28676). Labelled samples were run on an Applied Biosystems 3500/3500xL Genetic Analyzer and analysed with GlycanAssure Data Acquisition Software (v1.0) and Microsoft Excel (v16.43).

Human research participants
Primary cells used in select in vitro assays were from the blood of healthy human immunodeficiency virus (HIV)-negative participants. Participants were recruited through a voluntary donation program conducted at Massachusetts General Hospital. Participants were informed about the study through informational sessions and written materials, and those interested underwent screening for eligibility.

Eligibility criteria included the absence of clinical signs of illness and negative test results for active HIV, hepatitis C virus and hepatitis B virus infections. The samples were provided by individuals who did not have any role in the research study. The specimens were provided anonymized or coded. Information on sex, gender, age, race, ethnicity or other socially relevant groupings was not available to investigators. All donors provided written, informed consent. The study was approved by the institutional review board at Massachusetts General Hospital under protocol number 2010P002121.

ADCP

ADCP was performed following established protocols[56,64], with slight modifications. About 250 µg of *Mtb* H37Rv whole-cell lysate (BEI, NR-14822) was first treated with sodium acetate (25 µl NaOAc at 1 M and pH 5.5) and sodium periodate (55 µl NaIO₄ at 50 mM) and incubated for 90 min at room temperature in the dark. Next, sodium bisulfate (30 µl NaHSO₄ at 0.8 M and diluted in 0.1 M NaOAc) was added to block the oxidation reaction for 5 min at room temperature in the dark. The oxidized whole-cell lysate solution was transferred to a new tube; then 55 µl of hydrazide biotin at 50 mM (Sigma, 21339), 25 µl of 1 M NaOAc and 175 µl of ddH₂O were then added to the oxidized whole-cell lysate and incubated for 2 h at room temperature. Following the incubation, excess biotin was removed using Amicon Ultra 0.5 L columns (3 K, Millipore Sigma). The biotinylated whole-cell lysate was then added to FITC neutravidin beads (Thermo Fisher, F8776) at a ratio of 5 µg antigen:1 µl beads and incubated shaking overnight at 4 °C. Whole-cell lysate-coated beads were centrifuged at 16,000 *g* for 5 min, resuspended in 1 ml 5% BSA–PBS, and incubated shaking at room temperature for 1 h to block. Whole-cell lysate-coated beads were then resuspended in 5% BSA–PBS such that the starting 1 µl of beads were in 100 µl of solution. A 10 µl volume of whole-cell lysate-coated beads were then incubated with 40 µl of each monoclonal antibody at 0.025 µg ml⁻¹ (1 µg antibody total) for 2 h at 37 °C to form immune complexes. Human IgG1 isotype control antibody was used as negative control (Immune Technology, IT-001-37G12). After the immune complexes were washed with PBS, THP-1 monocytes (5.0 × 10⁴ per well) were added and incubated with the immune complexes for 16 h at 37 °C. Fluorescent bead uptake was measured in 4% paraformaldehyde (PFA) fixed cells by flow cytometry on a BD LSRII (BD Biosciences) and analysed by FlowJo 10.3 (Supplementary Fig. 2a). Phagocytic scores were calculated as follows: ((%FITC positive cells) × (geometric mean fluorescence intensity of the FITC positive cells))/10,000. Samples were run twice in technical duplicate, and results were averaged across two independent runs.

ADNP

ADNP was performed following established protocols[56,65], with minor modifications. *Mtb* H37Rv whole-cell lysate was oxidized, biotinylated, coupled to FITC neutravidin beads (Thermo Fisher, F8776), incubated with antibody and washed as described in the previous section for ADCP. Human IgG1 isotype control antibody was used as negative control (Immune Technology, IT-001-37G12). Next, fresh blood collected from healthy donors in acid citrate dextrose anti-coagulant tubes was added at a 1:9 ratio to ACK lysis buffer (Quality Biological, 10128-802) and incubated for 5 min at room temperature. Leukocytes were washed with PBS and resuspended in R10 medium–RPMI (Sigma), 10% fetal bovine serum (Sigma), 10 mM HEPES (Corning), 2 mM L-glutamine (Corning)–at a concentration of 2.5 × 10⁵ cells per ml. About 5 × 10⁴ leukocytes per well were added to the immune-complexed beads and incubated for 1 h at 37 °C. The cells were stained with anti-human CD66b-Pacific Blue (BioLegend) diluted to 1:250, washed with PBS and then fixed with 4% PFA. Bead uptake was measured by flow cytometry on a BD LSRII (BD Biosciences) and analysed by FlowJo 10.3 (Supplementary Fig. 2b). Phagocytic scores were calculated in the CD66b positive cell population. Samples were run twice in technical

duplicate, and results were averaged across two independent runs using distinct blood donors.

ADCD

ADCD was performed following an established protocol[66], with minor modifications. *Mtb* H37Rv whole-cell lysate was oxidized, biotinylated, coupled to red fluorescent neutravidin beads (Thermo Fisher, F8775), incubated with antibody and washed as described in the 'ADCP' section. Human IgG1 isotype control antibody was used as negative control (Immune Technology, IT-001-37G12). Next, guinea pig complement (Cedarlane, CL4051) diluted in magnesium- and calcium-containing veronal buffer (Boston Bioproducts) was added to the immune-complexed beads and incubated for 20 min at 37 °C. Beads were then washed in 15 mM EDTA–PBS and stained with FITC-conjugated anti-guinea pig C3 antibody (MP Biomedicals, MP0855385) diluted to 1:100. C3 deposition onto beads (FITC MFI of all beads) was evaluated by flow cytometry on a BD LSRII (BD Biosciences) and analysed by FlowJo 10.3 (Supplementary Fig. 2c). Samples were run twice in technical duplicate, and results were averaged across two independent runs.

ADNKA

ADNKA was performed following an established protocol[56], with minor modifications. ELISA plates (Thermo Fisher, NUNC MaxiSorp flat bottom) were coated with 250 ng per well of bovine liver glycogen (Milipore Sigma, G0885) overnight at 4 °C. The plates were washed with PBS and blocked with 5% BSA–PBS at room temperature for 2 h. The plates were washed with PBS, and 40 µl of each monoclonal antibody at 0.025 µg ml⁻¹ (1 µg antibody total) was added and incubated for 2 h at 37 °C. Human IgG1 isotype control antibody was used as negative control (Immune Technology, IT-001-37G12). One day before adding antibody, NK cells were isolated from healthy human donors using the RosetteSep human NK cell enrichment cocktail (Stemcell, 15065) and incubated overnight at 1.5 × 10⁶ cells per ml in R10 media with 1 ng ml⁻¹ of IL-15 (Stemcell) at 37 °C. After the 2 h incubation on the day of the assay, the ELISA assay plates were washed with PBS, and 50,000 NK cells, 2.5 µl PE-Cy5 anti-human CD107a (BD), 10 µl GolgiStop (BD) and 0.4 µl Brefeldin A (5 mg ml⁻¹, Sigma) were added to each well. The ELISA assay plates were incubated for 5 h at 37 °C. After the incubation, cells were stained for surface expression with Alexa Fluor 700 anti-human CD3 diluted to 1:40, PE-Cy7 anti-human CD56 diluted to 1:10 and APC-Cy7 anti-human CD16 diluted to 1:10 (all from BD). The cells were washed with PBS and then fixed using Perm A and Perm B (Invitrogen). The Perm B solution contained PE anti-human MIP-1β diluted to 1:50 and FITC anti-human IFNγ diluted to 1:20 (both from BD) for intracellular cytokine staining. The cells were washed, and the fluorescence of each marker was measured on a BD LSR II flow cytometer (BD Biosciences) and analysed by FlowJo 10.3 (Supplementary Fig. 2d). Samples were run twice in technical duplicate, and results were averaged across two distinct NK cell donors.

Macrophage restriction assay

In vitro macrophage *Mtb* survival was measured following established protocols[17,56], with slight modifications. CD14 positive cells were isolated from healthy donors using the EasySep CD14 Selection Kit II (Stemcell). CD14 positive cells were matured for 7 days into human MDMs in R10 media without phenol in low adherent flasks (Corning) and then plated at 50,000 cells per well in glass-bottom, 96-well plates (Greiner) 24 h before infection. *Mtb* H37Rv with constitutive mCherry and anhydrotetracycline inducible green fluorescent protein (GFP) expression (*Mtb-live/dead*)[24] was cultured in log phase and filtered through a 5 µm filter (Milliplex) before MDM infection at a multiplicity of infection of 1 overnight at 37 °C. Infected MDMs were washed with PBS. Then, 200 µl of monoclonal antibody at 50 µg ml⁻¹ in R10 without phenol was added, and the mixture was incubated at 37 °C. Human IgG1

isotype control antibody was used as negative control (Immune Technology, IT-001-37G12). Three days after infection, anhydrotetracycline (Sigma) was added to the infected MDMs at 200 ng ml^{-1}, which was then incubated for 16 h at 37 °C. Cells were then fixed with 4% PFA and stained with DAPI. Data were analysed using the Columbus Image Data Storage and Analysis System. *Mtb* survival was calculated as the ratio of live to total bacteria within macrophages in each well. *Mtb* survival for each condition was normalized by *Mtb* survival in the no-antibody condition. The assay was performed in technical triplicate and in MDMs from two donors.

WBA

Whole blood from healthy human donors was collected the day of the experiment in acid citrate dextrose anti-coagulant tubes. An auto-luminescent H37Rv *Mtb* reporter strain (*Mtb-276*)[25] was cultured in log phase, washed and then resuspended in R10 without phenol. Whole blood was simultaneously infected with *Mtb-276* at 1.0×10^6 bacteria per ml of blood and treated with antibody in a white, flat-bottom 96-well plate (Greiner) in a 1:1 ratio (150 µl blood and 150 µl of diluted antibody). The final concentration of antibody treatments was 25 µg ml^{-1} in 300 µl total. Human IgG1 isotype control antibody was used as negative control (BioXcell, BE0297). The final concentration of rifampin (Sigma) positive control was 0.25 µg ml^{-1}. At each time point—immediately after infection and every 24 h post infection until 120 h—the samples in each well were mixed, and a luminescence reading was taken (Tecan Spark 10M) to generate *Mtb* growth curves in the presence of each treatment. *Mtb* restriction in whole blood was calculated as the area under the curve for each condition. Area-under-the-curve values were computed in GraphPad Prism (version 8.4.0). The assay was performed in technical triplicate and in blood from multiple donors.

Blood immune cell depletions

StraightFrom Whole Blood CD66b (Miltenyi, 130-104-913), CD14 (Miltenyi, 130-090-879) or Basic unconjugated (Miltenyi, 130-048-001) microbeads were first buffer exchanged into 2 mM EDTA–PBS. Specifically, a Whole Blood Column (Miltenyi, 130-093-545) was attached to the MidiMacs (Miltenyi) and primed with 3 ml of separation buffer (PBS with 0.5% BSA and 2 mM EDTA). About 2 ml of microbeads was added to the primed Whole Blood Column, and the flow-through was discarded. After washing the column three times with 500 µl of PBS, the microbeads were eluted with a final volume of 1 ml in 2 mM EDTA–PBS. On the day of the assay, whole blood from healthy human donors was collected in acid citrate dextrose anti-coagulant tubes. About 100 µl of microspheres was added per millilitre of blood, and the solution was incubated for 20 min at 4 °C. During the incubation, Whole Blood Columns were attached to the MidiMacs and primed with 3 ml of separation buffer followed by 3 ml of R10 media. Following the incubation, the microsphere-treated blood was added to the column, and the flow-through was collected and used in the WBA described in the previous section.

Blood cytokine blockade and complement inhibition

To conduct cytokine blockade experiments, whole blood was collected from healthy human donors on the day of the experiment in acid citrate dextrose anti-coagulant tubes. Anti-IL-1β (Invivogen, clone 4H5) or anti-IFNγ (BioLegend, clone B27) was then added to the blood at 1 µg ml^{-1}. The blood treated with blocking antibodies was then used in the WBA as described above. For complement inhibition experiments, whole blood was collected from healthy human donors on the day of the experiment in acid citrate dextrose anti-coagulant tubes. Cobra venom factor (Sigma, 233552-M) was added to the blood at a concentration of 50 µg ml^{-1}, and the mixture was incubated at 37 °C for 1 h to inactivate complement[67]. Following complement inhibition, the cobra venom factor-treated blood was used in the WBA as described above.

Cytokine Luminex

At the final time point of the WBA (120 h), the assay plates were centrifuged at 800 *g* for 5 min; then 110 µl of the supernatant was collected from each well and transferred into a separate 96-well plate which was stored at −20 °C until further use. Supernatants were thawed and twice filtered using 0.2 µm 96-well filter plates (Millipore Sigma, CLS3508) for removal from the biosafety level 3 laboratory space. The abundance of select cytokines was then measured in 50 µl of the supernatants with a Human Cytokine Magnetic 10-Plex Panel (Thermo Fisher, LHC0001M) according to the instructions of the manufacturer. The median fluorescence intensity (MFI) for each analyte was measured using a FlexMap 3D (Luminex). Samples were measured in technical triplicate in blood from two donors.

scRNA-seq

Whole-blood *Mtb* infection and the addition of antibody was performed as described above for the WBA. Blood from three healthy donors was used. Twenty-four hours following infection and the addition of antibody, blood from each donor was added at a 1:9 ratio to ACK lysis buffer (Quality Biological, 10128-802) and incubated for 10 min at room temperature. Cells were centrifuged at 400 *g* for 5 min, and the supernatant was discarded. About 10 ml of ACK lysis buffer was added to the cell pellet to repeat the lysis procedure. Cells were centrifuged at 400 *g* for 5 min, and the supernatant was discarded. Samples were washed twice with PBS buffer and counted before multiplexing using lipid-tagged indices (MULTI)-seq barcoding following an established protocol[68]. In brief, samples were barcoded with 2.5 µM of the lipid-modified oligonucleotide (LMO) anchor and barcode for 5 min on ice in PBS before adding 2.5 µM of the LMO co-anchor and incubating for an additional 5 min. Samples were quenched with 1% BSA in PBS and washed once. Samples were pooled, and 0.5 U µl^{-1} RNase inhibitor (Roche) was added. Pooled samples were then loaded into two lanes using the 10X Genomics NextGEM Single Cell 3′ kit v3.1 per the manufacturer's protocol. Complementary DNA was inactivated at 95 °C for 15 min before biosafety level 3 removal for library construction. Libraries were sequenced on a NextSeq500 (Illumina). FASTQ files were processed using CellRanger v6.1.2 to generate gene expression count matrices and deMULTIplex to generate LMO barcode count matrices.

scRNA-seq data analysis

LMO barcode and gene expression count matrices were analysed using R (v4.0.3) and Seurat (v4.0.0). Cells were identified using emptyDrops (DropletUtils) and were demuxed using HTODemux (Seurat) and hashedDrops (DropletUtils). Each lane was subject to demultiplexing and quality control separately and then merged for downstream analyses. Cells with less than 300 unique genes detected were excluded. Additional cells were excluded based on the assessment of cluster-specific technical metrics (percentage of mitochondrial reads per cell and number of unique molecular identifiers per cell). Counts were normalized using the default parameters from NormalizeData (Seurat), for example, scaling by 10,000 and log normalization. Three thousand variable features were used for principal component analysis (PCA). Smart local moving clustering was performed using FindClusters (Seurat) on the shared nearest neighbour graph generated from FindNeighbors (Seurat) using 30 principal components and $k = 20$. Cell-type annotation was based on expert annotation and predicted cell type labels from the peripheral blood mononuclear cell dataset in Azimuth using FindTransferAnchors and TransferData (Seurat). Marker gene statistics were calculated using wilcoxauc (presto). Genes consistently increased following 24c5 SEHFST LS antibody treatment were defined as those: (1) with a Mann–Whitney $P < 0.1$ and a $\log_2$ fold change greater than 0.25 compared with either the 24c5 IgG1 or no Ab condition, (2) detected in a minimum fraction of 0.1 cells in either of the two conditions and (3) with a $\log_2$ fold change greater than 0 compared with both the 24c5 IgG1 and no Ab conditions. Genes consistently decreased following 24c5 SEHFST LS antibody treatment were defined

as those: (1) with a Mann–Whitney $P < 0.1$ and a $\log_2$ fold change less than -0.25 compared with either the 24c5 IgG1 or no Ab conditions, (2) detected in a minimum fraction of 0.1 cells in either of the two conditions and (3) a $\log_2$ fold change less than 0 compared with both the 24c5 IgG1 and no Ab conditions.

GO analysis

GO analysis was performed using the Enrichr web-based platform[69]. Input genes for the 24c5 SEHFST LS positive enrichment analysis included genes consistently increased following 24c5 SEHFST LS antibody treatment compared with both the 24c5 IgG1 and the no Ab conditions (Fig. 6c, red quadrant). Input genes for the 24c5 SEHFST LS negative enrichment analysis included genes consistently decreased following 24c5 SEHFST LS antibody treatment compared with both the 24c5 IgG1 and the no Ab conditions (Fig. 6c, blue quadrant). Gene Ontology Biological Process was the gene set source. Top 10 gene sets ranked by Benjamini–Hochberg adjusted P value are shown[70]. Gene sets with an adjusted $P < 0.05$ were considered significant.

Multivariate analyses

Complete-linkage hierarchical clustering was performed on the z-scored antibody functional data using the SciPy library in Python (version 3.8.8). Polar plots were generated on the max-normalized antibody functional data using the ggplot2 (version 3.3.5) package in R (version 4.1.1). Clustered heat maps of the z-scored antibody functional data were generated using the gplots (version 3.1.1) package in R (version 4.1.1). PCA on the z-scored cytokine data was performed using the factoextra (version 1.0.7) and ggplot2 (version 3.3.5) packages in R (version 4.1.1). Spearman correlations analyses were performed using the corrplot (version 0.92) package in R (version 4.1.1) and visualized using the corrplot (version 0.92) and ggpubr (version 0.4.0) packages in R (version 4.1.1).

Statistics

For the macrophage restriction assay, WBA and cytokine Luminex assay, one-way analysis of variance (ANOVA) tests were implemented with Dunnett's correction comparing each antibody with the isotype IgG1 control antibody. For the blood immune cell depletion assays and complement inhibition assay, two-tailed, unpaired t-tests were performed, comparing restriction in the immune cell depleted blood condition with the whole-blood condition for each treatment. These statistics were performed in GraphPad Prism (version 8.4.0). Spearman correlations between antibody functional assays were computed in R (version 4.1.1).

Reporting summary

Further information on research design is available in the Nature Portfolio Reporting Summary linked to this article.

Data availability

RNA-seq data have been deposited in the Gene Expression Omnibus under accession number GSE271079. Source data are provided with this paper. All other data and metadata associated with this study are available in the main text, Supplementary Information and/or at https://fairdomhub.org/studies/1089.

Code availability

Scripts to perform the computational analyses presented in the paper are available via GitHub at https://github.com/eirvine94/tb_fc_engineering_manuscript. The code is also available via Zenodo at https://doi.org/10.5281/zenodo.11282075 (ref. 71).

References

1. *Global Tuberculosis Report* (World Health Organization, 2023).
2. Caruso, A. M. et al. Mice deficient in CD4 T cells have only transiently diminished levels of IFN-gamma, yet succumb to tuberculosis. *J. Immunol.* **162**, 5407–5416 (1999).
3. Lin, P. L. et al. CD4 T cell depletion exacerbates acute *Mycobacterium tuberculosis* while reactivation of latent infection is dependent on severity of tissue depletion in cynomolgus macaques. *AIDS Res. Hum. Retroviruses* **28**, 1693–1702 (2012).
4. Diedrich, C. R. et al. Reactivation of latent tuberculosis in cynomolgus macaques infected with SIV is associated with early peripheral T cell depletion and not virus load. *PLoS ONE* **5**, e9611 (2010).
5. Maglione, P. J., Xu, J. & Chan, J. B cells moderate inflammatory progression and enhance bacterial containment upon pulmonary challenge with *Mycobacterium tuberculosis*. *J. Immunol.* **178**, 7222–7234 (2007).
6. Hamasur, B. et al. A mycobacterial lipoarabinomannan specific monoclonal antibody and its F(ab') fragment prolong survival of mice infected with *Mycobacterium tuberculosis*. *Clin. Exp. Immunol.* **138**, 30–38 (2004).
7. Teitelbaum, R. et al. A mAb recognizing a surface antigen of *Mycobacterium tuberculosis* enhances host survival. *Proc. Natl Acad. Sci. USA* **95**, 15688–15693 (1998).
8. Pethe, K. et al. The heparin-binding haemagglutinin of *M. tuberculosis* is required for extrapulmonary dissemination. *Nature* **412**, 190–194 (2001).
9. Balu, S. et al. A novel human IgA monoclonal antibody protects against tuberculosis. *J. Immunol.* **186**, 3113–3119 (2011).
10. Watson, A. et al. Human antibodies targeting a *Mycobacterium* transporter protein mediate protection against tuberculosis. *Nat. Commun.* **12**, 602 (2021).
11. Li, H. et al. Latently and uninfected healthcare workers exposed to TB make protective antibodies against *Mycobacterium tuberculosis*. *Proc. Natl Acad. Sci. USA* **114**, 5023–5028 (2017).
12. Chen, T. et al. Capsular glycan recognition provides antibody-mediated immunity against tuberculosis. *J. Clin. Invest.* **130**, 1808–1822 (2020).
13. Krishnananthasivam, S. et al. An anti-LpqH human monoclonal antibody from an asymptomatic individual mediates protection against *Mycobacterium tuberculosis*. *npj Vaccines* **8**, 127 (2023).
14. Chen, T. et al. Association of human antibodies to arabinomannan with enhanced mycobacterial opsonophagocytosis and intracellular growth reduction. *J. Infect. Dis.* **214**, 300–310 (2016).
15. Prados-Rosales, R. et al. Enhanced control of *Mycobacterium tuberculosis* extrapulmonary dissemination in mice by an arabinomannan–protein conjugate vaccine. *PLoS Pathog.* **13**, e1006250 (2017).
16. Maglione, P. J., Xu, J., Casadevall, A. & Chan, J. Fc gamma receptors regulate immune activation and susceptibility during *Mycobacterium tuberculosis* infection. *J. Immunol.* **180**, 3329–3338 (2008).
17. Lu, L. L. et al. A functional role for antibodies in tuberculosis. *Cell* **167**, 433–443.e14 (2016).
18. Sani, M. et al. Direct visualization by cryo-EM of the mycobacterial capsular layer: a labile structure containing ESX-1-secreted proteins. *PLoS Pathog.* **6**, e1000794 (2010).
19. Lemassu, A. & Daffé, M. Structural features of the exocellular polysaccharides of *Mycobacterium tuberculosis*. *Biochem. J.* **297**, 351–357 (1994).
20. Ortalo-Magné, A. et al. Molecular composition of the outermost capsular material of the tubercle bacillus. *Microbiology* **141**, 1609–1620 (1995).
21. Schwebach, J. R. et al. Glucan is a component of the *Mycobacterium tuberculosis* surface that is expressed in vitro and in vivo. *Infect. Immun.* **70**, 2566–2575 (2002).
22. Keitel, W. A. et al. Effects of infection and disease with *Mycobacterium tuberculosis* on serum antibody to glucan and arabinomannan: two surface polysaccharides of this pathogen. *BMC Infect. Dis.* **13**, 276 (2013).

23. Yu, X. et al. Comparative evaluation of profiles of antibodies to mycobacterial capsular polysaccharides in tuberculosis patients and controls stratified by HIV status. *Clin. Vaccine Immunol.* **19**, 198–208 (2012).

24. Martin, C. J. et al. Efferocytosis is an innate antibacterial mechanism. *Cell Host Microbe* **12**, 289–300 (2012).

25. Andreu, N. et al. Optimisation of bioluminescent reporters for use with mycobacteria. *PLoS ONE* **5**, e10777 (2010).

26. Gunn, B. M. et al. A Fc engineering approach to define functional humoral correlates of immunity against Ebola virus. *Immunity* **54**, 815–828.e5 (2021).

27. Smith, P., DiLillo, D. J., Bournazos, S., Li, F. & Ravetch, J. V. Mouse model recapitulating human Fcγ receptor structural and functional diversity. *Proc. Natl Acad. Sci. USA* **109**, 6181–6186 (2012).

28. Shields, R. L. et al. High resolution mapping of the binding site on human IgG1 for Fc gamma RI, Fc gamma RII, Fc gamma RIII, and FcRn and design of IgG1 variants with improved binding to the Fc gamma R. *J. Biol. Chem.* **276**, 6591–6604 (2001).

29. Lazar, G. A. et al. Engineered antibody Fc variants with enhanced effector function. *Proc. Natl Acad. Sci. USA* **103**, 4005–4010 (2006).

30. Idusogie, E. E. et al. Engineered antibodies with increased activity to recruit complement. *J. Immunol.* **166**, 2571–2575 (2001).

31. Moore, G. L., Chen, H., Karki, S. & Lazar, G. A. Engineered Fc variant antibodies with enhanced ability to recruit complement and mediate effector functions. *MAbs* **2**, 181–189 (2010).

32. Richards, J. O. et al. Optimization of antibody binding to FcgammaRIIa enhances macrophage phagocytosis of tumor cells. *Mol. Cancer Ther.* **7**, 2517–2527 (2008).

33. Masuda, K. et al. Enhanced binding affinity for FcgammaRIIIa of fucose-negative antibody is sufficient to induce maximal antibody-dependent cellular cytotoxicity. *Mol. Immunol.* **44**, 3122–3131 (2007).

34. Stapleton, N. M. et al. Competition for FcRn-mediated transport gives rise to short half-life of human IgG3 and offers therapeutic potential. *Nat. Commun.* **2**, 599 (2011).

35. Tao, M. H. & Morrison, S. L. Studies of aglycosylated chimeric mouse-human IgG. Role of carbohydrate in the structure and effector functions mediated by the human IgG constant region. *J. Immunol.* **143**, 2595–2601 (1989).

36. Walker, M. R., Lund, J., Thompson, K. M. & Jefferis, R. Aglycosylation of human IgG1 and IgG3 monoclonal antibodies can eliminate recognition by human cells expressing Fc gamma RI and/or Fc gamma RII receptors. *Biochem. J* **259**, 347–353 (1989).

37. Zalevsky, J. et al. Enhanced antibody half-life improves in vivo activity. *Nat. Biotechnol.* **28**, 157–159 (2010).

38. Dall'Acqua, W. F. et al. Increasing the affinity of a human IgG1 for the neonatal Fc receptor: biological consequences. *J. Immunol.* **169**, 5171–5180 (2002).

39. Vogel, C.-W., Fritzinger, D. C., Hew, B. E., Thorne, M. & Bammert, H. Recombinant cobra venom factor. *Mol. Immunol.* **41**, 191–199 (2004).

40. Kroon, E. E. et al. Neutrophils: innate effectors of TB resistance? *Front. Immunol.* **9**, 2637 (2018).

41. Lowe, D. M., Redford, P. S., Wilkinson, R. J., O'Garra, A. & Martineau, A. R. Neutrophils in tuberculosis: friend or foe? *Trends Immunol.* **33**, 14–25 (2012).

42. Eruslanov, E. B. et al. Neutrophil responses to *Mycobacterium tuberculosis* infection in genetically susceptible and resistant mice. *Infect. Immun.* **73**, 1744–1753 (2005).

43. Dallenga, T. & Schaible, U. E. Neutrophils in tuberculosis—first line of defence or booster of disease and targets for host-directed therapy? *Pathog. Dis.* **74**, ftw012 (2016).

44. Lowe, D. M. et al. Differential effect of viable versus necrotic neutrophils on *Mycobacterium tuberculosis* growth and cytokine induction in whole blood. *Front. Immunol.* **9**, 903 (2018).

45. Baranger, K., Zani, M.-L., Chandenier, J., Dallet-Choisy, S. & Moreau, T. The antibacterial and antifungal properties of trappin-2 (pre-elafin) do not depend on its protease inhibitory function. *FEBS J.* **275**, 2008–2020 (2008).

46. Bellemare, A., Vernoux, N., Morin, S., Gagné, S. M. & Bourbonnais, Y. Structural and antimicrobial properties of human pre-elafin/trappin-2 and derived peptides against *Pseudomonas aeruginosa*. *BMC Microbiol.* **10**, 253 (2010).

47. Mesquita, G. et al. H-Ferritin is essential for macrophages' capacity to store or detoxify exogenously added iron. *Sci. Rep.* **10**, 3061 (2020).

48. Sanchez-Niño, M. D. et al. BASP1 promotes apoptosis in diabetic nephropathy. *J. Am. Soc. Nephrol.* **21**, 610–621 (2010).

49. Carpenter, B. et al. BASP1 is a transcriptional cosuppressor for the Wilms' tumor suppressor protein WT1. *Mol. Cell. Biol.* **24**, 537–549 (2004).

50. Waldera-Lupa, D. M. et al. Proteome-wide analysis reveals an age-associated cellular phenotype of in situ aged human fibroblasts. *Aging* **6**, 856–878 (2014).

51. Amulic, B., Cazalet, C., Hayes, G. L., Metzler, K. D. & Zychlinsky, A. Neutrophil function: from mechanisms to disease. *Annu. Rev. Immunol.* **30**, 459–489 (2012).

52. Nordenfelt, P. & Tapper, H. Phagosome dynamics during phagocytosis by neutrophils. *J. Leukoc. Biol.* **90**, 271–284 (2011).

53. Boelaert, J. R., Vandecasteele, S. J., Appelberg, R. & Gordeuk, V. R. The effect of the host's iron status on tuberculosis. *J. Infect. Dis.* **195**, 1745–1753 (2007).

54. Tran, A. C. et al. Mucosal therapy of multi-drug resistant tuberculosis with IgA and interferon-γ. *Front. Immunol.* **11**, 582833 (2020).

55. Zimmermann, N. et al. Human isotype-dependent inhibitory antibody responses against *Mycobacterium tuberculosis*. *EMBO Mol. Med.* **8**, 1325–1339 (2016).

56. Irvine, E. B. et al. Robust IgM responses following intravenous vaccination with Bacille Calmette-Guérin associate with prevention of *Mycobacterium tuberculosis* infection in macaques. *Nat. Immunol.* **22**, 1515–1523 (2021).

57. Xu, D. et al. In vitro characterization of five humanized OKT3 effector function variant antibodies. *Cell. Immunol.* **200**, 16–26 (2000).

58. Kimmey, J. M. et al. Unique role for ATG5 in neutrophil-mediated immunopathology during *M. tuberculosis* infection. *Nature* **528**, 565–569 (2015).

59. Moreira-Teixeira, L. et al. Type I IFN exacerbates disease in tuberculosis-susceptible mice by inducing neutrophil-mediated lung inflammation and NETosis. *Nat. Commun.* **11**, 5566 (2020).

60. Lu, L. L. et al. Antibody Fc glycosylation discriminates between latent and active tuberculosis. *J. Infect. Dis.* **222**, 2093–2102 (2020).

61. Zhang, X., Majlessi, L., Deriaud, E., Leclerc, C. & Lo-Man, R. Coactivation of Syk kinase and MyD88 adaptor protein pathways by bacteria promotes regulatory properties of neutrophils. *Immunity* **31**, 761–771 (2009).

62. Engler, C. & Marillonnet, S. Golden Gate cloning. *Methods Mol. Biol.* **1116**, 119–131 (2014).

63. Fang, J. et al. Stable antibody expression at therapeutic levels using the 2A peptide. *Nat. Biotechnol.* **23**, 584–590 (2005).

64. Ackerman, M. E. et al. A robust, high-throughput assay to determine the phagocytic activity of clinical antibody samples. *J. Immunol. Methods* **366**, 8–19 (2011).

65. Karsten, C. B. et al. A versatile high-throughput assay to characterize antibody-mediated neutrophil phagocytosis. *J. Immunol. Methods* **471**, 46–56 (2019).

66. Fischinger, S. et al. A high-throughput, bead-based, antigen-specific assay to assess the ability of antibodies to induce complement activation. *J. Immunol. Methods* **473**, 112630 (2019).

67. Swartz, R. P., Naai, D., Vogel, C. W. & Yeager, H. Jr. Differences in uptake of mycobacteria by human monocytes: a role for complement. *Infect. Immun.* **56**, 2223–2227 (1988).

68. McGinnis, C. S. et al. MULTI-seq: sample multiplexing for single-cell RNA sequencing using lipid-tagged indices. *Nat. Methods* **16**, 619–626 (2019).

69. Chen, E. Y. et al. Enrichr: interactive and collaborative HTML5 gene list enrichment analysis tool. *BMC Bioinformatics* **14**, 128 (2013).

70. Benjamini, Y. & Hochberg, Y. Controlling the false discovery rate: a practical and powerful approach to multiple testing. *J. R. Stat. Soc.* **57**, 289–300 (1995).

71. Irvine, E. B. eirvine94/tb_fc_engineering_manuscript: release v1.0. *Zenodo* https://doi.org/10.5281/zenodo.11282075 (2024).

72. Asokan, M. et al. Fc-mediated effector function contributes to the in vivo antiviral effect of an HIV neutralizing antibody. *Proc. Natl Acad. Sci. USA* **117**, 18754–18763 (2020).

73. Petkova, S. B. et al. Enhanced half-life of genetically engineered human IgG1 antibodies in a humanized FcRn mouse model: potential application in humorally mediated autoimmune disease. *Int. Immunol.* **18**, 1759–1769 (2006).

74. Hinton, P. R. et al. Engineered human IgG antibodies with longer serum half-lives in primates. *J. Biol. Chem.* **279**, 6213–6216 (2004).

75. Grevys, A. et al. Fc Engineering of human IgG1 for altered binding to the neonatal Fc receptor affects Fc effector functions. *J. Immunol.* **194**, 5497–5508 (2015).

76. Datta-Mannan, A. et al. Humanized IgG1 variants with differential binding properties to the neonatal Fc receptor: relationship to pharmacokinetics in mice and primates. *Drug Metab. Dispos.* **35**, 86–94 (2007).

77. Yeung, Y. A. et al. Engineering human IgG1 affinity to human neonatal Fc receptor: impact of affinity improvement on pharmacokinetics in primates. *J. Immunol.* **182**, 7663–7671 (2009).

78. Datta-Mannan, A., Witcher, D. R., Tang, Y., Watkins, J. & Wroblewski, V. J. Monoclonal antibody clearance. Impact of modulating the interaction of IgG with the neonatal Fc receptor. *J. Biol. Chem.* **282**, 1709–1717 (2007).

79. Chu, S. Y. et al. Inhibition of B cell receptor-mediated activation of primary human B cells by coengagement of CD19 and FcgammaRIIb with Fc-engineered antibodies. *Mol. Immunol.* **45**, 3926–3933 (2008).

80. Diebolder, C. A. et al. Complement is activated by IgG hexamers assembled at the cell surface. *Science* **343**, 1260–1263 (2014).

81. Wirt, T. et al. An Fc double-engineered CD20 antibody with enhanced ability to trigger complement-dependent cytotoxicity and antibody-dependent cell-mediated cytotoxicity. *Transfus. Med. Hemother.* **44**, 292–300 (2017).

Acknowledgements

Author contributions

E.B.I., R.L., P.S.G., S.M.F. and G.A. were responsible for the conceptualization of the study. The methodology was developed by E.B.I., A.N., M.Z.K., J.M.P., R.L., P.S.G., J.S., J.C.H., S.M.F. and G.A. E.B.I. and J.M.P. handled the software aspects. Validation was performed by E.B.I., A.N., M.Z.K., A.W. and S.S. Formal analysis was conducted by E.B.I., A.N., M.Z.K., J.M.P. and P.S.G. The investigation was carried out by E.B.I., A.N., M.Z.K., J.M.P., P.S.G., J.S., S.S., W.K., J.C.H. and E.v.W. Resources were provided by A.W., S.S., W.K., A.C. and L.C. Data curation was managed by E.B.I., A.N., M.Z.K., J.M.P. and P.S.G. E.B.I. drafted the original manuscript, with all authors contributing to the review and editing process. Visualization was undertaken by E.B.I. The supervision of the project was carried out by B.D.B., L.C., S.M.F. and G.A. Project administration was managed by S.M.F. and G.A. Funding acquisition was secured by E.B.I., B.D.B., L.C., S.M.F. and G.A.

Competing interests

## Additional information

Extended Data Fig. 1 | See next page for caption.

Extended Data Fig. 1 | Functional profiling of Fc-engineered α-glucan antibodies. a, Glucan (bovine liver glycogen) antigen-binding ELISA of the α-glucan-specific Fc-variant panel. Area under the 5-point dilution curve is plotted. ELISA was run in technical duplicate. **b**, Heatmap of individual Fc glycan structures for each 24c5 Fc variant. **c**, Clustered heatmap indicating the performance of each α-glucan Fc-variant in the functional profiling assays. Data were z-scored prior to heatmap visualization. **d**, Spearman correlations of paired normal and half-life extended (LS) variants in the 24c5 Fc-variant panel. Spearman correlations were two-sided. Unadjusted p-values are indicated. **e**, Spearman correlation of functional profiling between an Fc-variant panel previously published Ebola-specific monoclonal antibody (VIC16) and the 24c5 α-glucan-specific Fc-variant panel. Spearman correlations were two-sided. Unadjusted p-values are indicated.
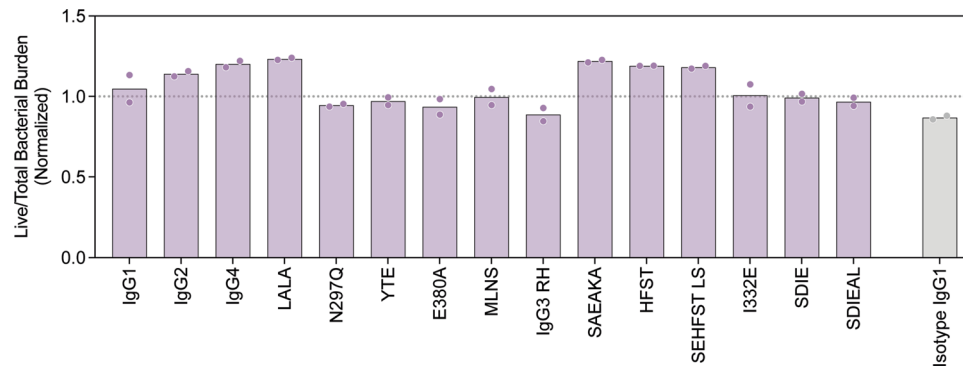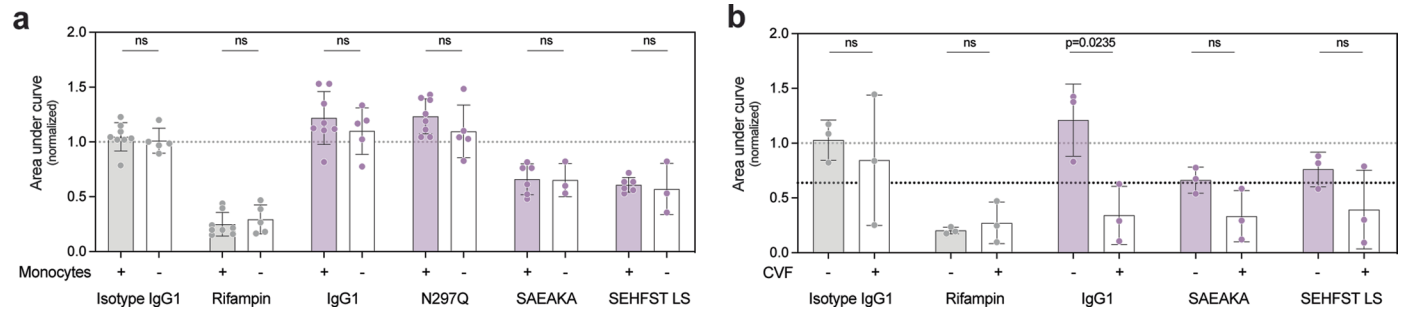
Extended Data Fig. 2 | Macrophage *Mtb* restriction assay of Fc-engineered α-glucan antibodies. Y-axis shows live (GFP) / total (mCherry) *Mtb* burden in human monocyte-derived macrophages normalized by the no antibody condition for the respective donor. Each point is the triplicate average from 1 human macrophage donor.
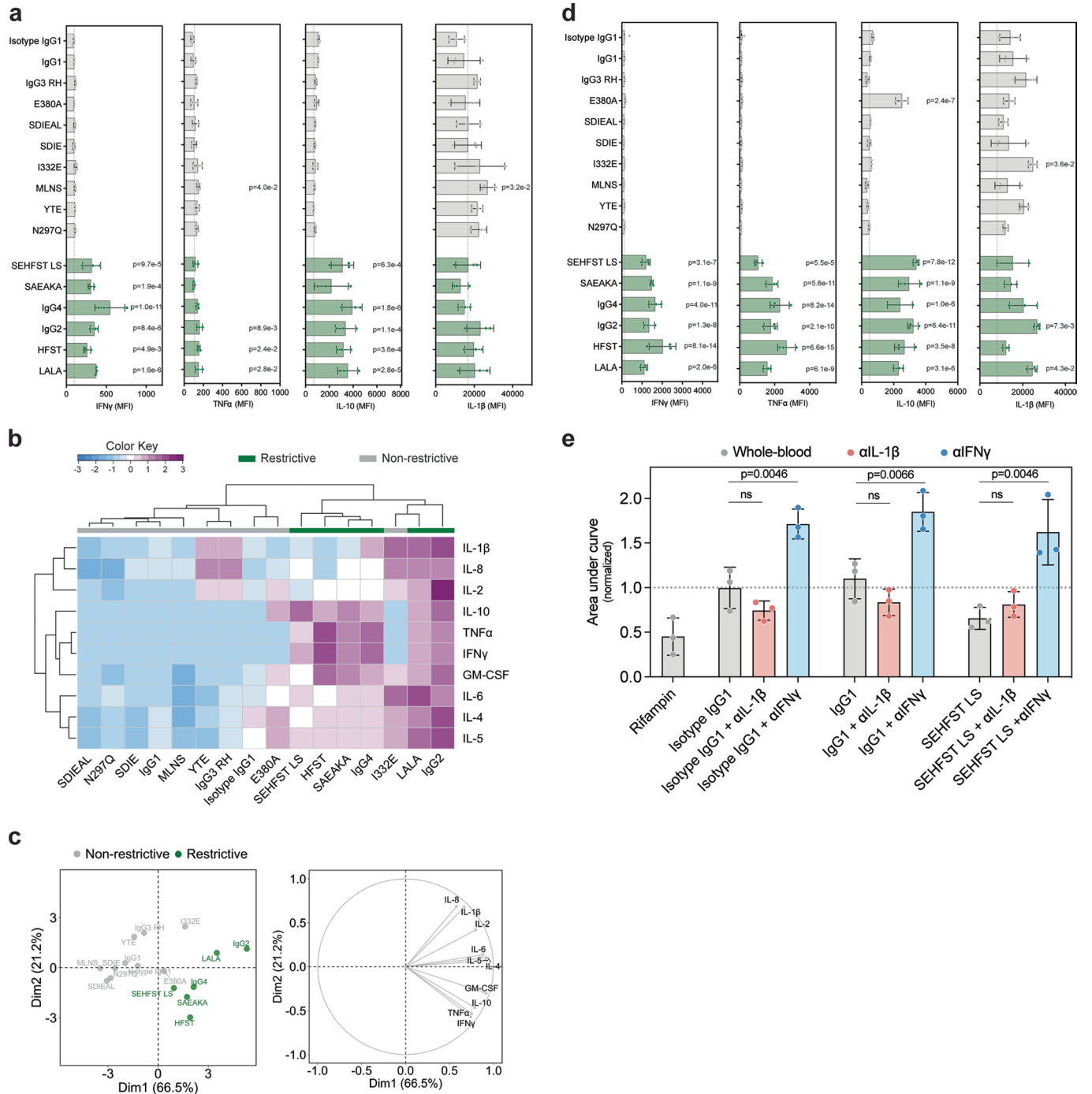
Extended Data Fig. 3 | Cytokine Luminex of whole-blood restriction assay.
Cytokine Luminex using the whole-blood assay supernatant collected at
120 hours. **a,d,** Luminex MFI across selected cytokines in **a**, Donor A, and **d**,
Donor B. One-way ANOVA with Dunnett's correction comparing each antibody
with the isotype IgG1 control antibody. Green (Restrictive); grey (Non-restrictive).
Adjusted p-values < 0.05 are shown. Error bars indicate mean with standard
deviation. Run in technical triplicate. **b**, Clustered heatmap indicating the
cytokine profile elicited by each α-glucan Fc-variant in Donor B. Data were
z-scored prior to heatmap visualization. **c**, Principal component analysis of

cytokine Luminex data from Donor B. Left, score plot of the first two principal
components. Right, loading plot of the first two principal components.
e, Cytokine blockade experiments. 24c5 variants were tested for their ability
promote *Mtb* restriction in whole-blood (grey), whole-blood with an IL-1β
blocking antibody (pink), or whole-blood with an IFNγ blocking antibody (blue).
One-way ANOVA with Dunnett's correction comparing restriction in the IL-1β and
IFNγ blockade conditions, with the whole-blood condition for each treatment.
Error bars indicate mean with standard deviation of 3 biological replicates from
distinct donors.

Extended Data Fig. 4 | Whole-blood *Mtb* restriction assay with monocyte depletions and complement inhibition. a, Monocyte depletions. Each antibody or antibiotic treatment was tested in whole-blood (filled in bars) and monocyte depleted blood (white bars). Grey dotted line indicates the no antibody condition. **b**, Complement inhibition using cobra venom factor (CVF). Each antibody or antibiotic treatment was tested in whole-blood (filled in bars) and CVF-treated blood (white bars). Grey dotted line indicates the no antibody condition. Black dotted line indicates the CVF-treated no antibody condition. **a,b**, X-axis shows selected α-glucan Fc-variants (25 μg/mL), an IgG1 isotype control antibody as a negative control (25 μg/mL), and the antibiotic rifampin as a positive control (0.25 μg/mL). Y-axis is the area under the *Mtb-276* growth curve value normalized by the no antibody condition from the respective donor. Each point represents a triplicate average from one donor. Two-tailed, unpaired t test, comparing restriction in the monocyte depleted or CVF-treated blood condition with the whole-blood condition. Unadjusted p-values < 0.05 are indicated are comparisons labeled as "ns" (not significant) have unadjusted p-values > 0.05. Error bars show mean with standard deviation.
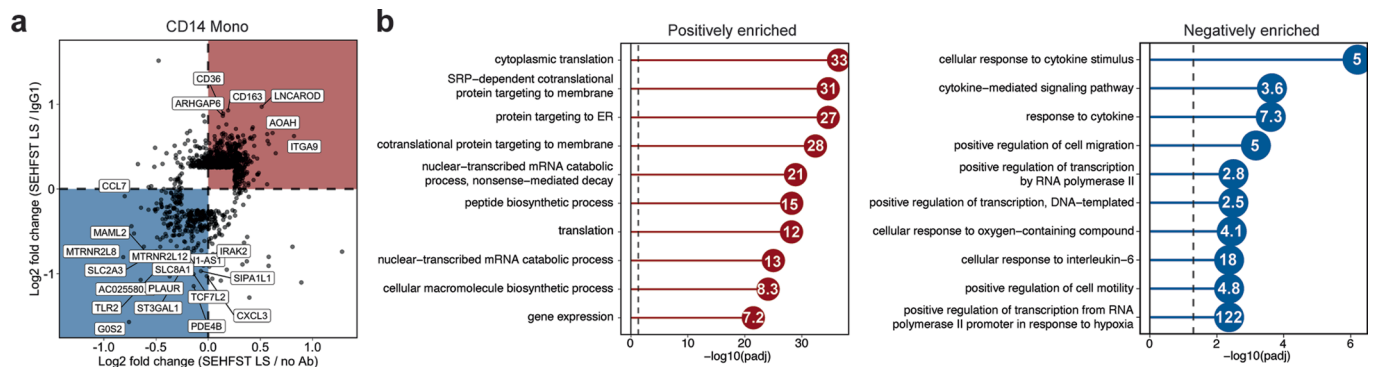
Extended Data Fig. 5 | CD14 monocyte differential expression analysis.
scRNAseq analysis of CD14 monocytes. **a**, Genes consistently increased in the
24c5 SEHFST LS condition (red quadrant): (i) Mann-Whitney p-value < 0.1 and a
log2 fold change > 0.25 compared to either the 24c5 IgG1 or no Ab condition,
(ii) detected in a minimum fraction of 0.1 cells in either of the two conditions, and
(iii) a log2 fold change > 0 compared to both the 24c5 IgG1 and no Ab conditions.
Genes consistently decreased in the 24c5 SEHFST LS condition (blue quadrant):
(i) Mann-Whitney p-value < 0.1 and a log2 fold change < −0.25 compared to either

the 24c5 IgG1 or no Ab conditions, (ii) detected in a minimum fraction of 0.1 cells
in either of the two conditions, and (iii) a log2 fold change < 0 compared to both
the 24c5 IgG1 and no Ab conditions. Mann-Whitney tests were two-sided. **b**, Gene
list enrichment analysis using GO Biological Process gene sets. Left, GO terms
enriched in red quadrant genes from panel C. Right, GO terms enriched in blue
quadrant genes from panel C. Vertical dashed line indicates two-sided Fisher's
exact test adjusted p-value of 0.05. Numbers on each circle show the odds ratio.
Top ten GO terms by Benjamini-Hochberg adjusted p-value shown.

Corresponding author(s): Sarah M. Fortune
Galit Alter

Last updated by author(s): July 2, 2024

Reporting Summary

Nature Portfolio wishes to improve the reproducibility of the work that we publish. This form provides structure for consistency and transparency in reporting. For further information on Nature Portfolio policies, see our Editorial Policies and the Editorial Policy Checklist.

Statistics

For all statistical analyses, confirm that the following items are present in the figure legend, table legend, main text, or Methods section.

n/a	Confirmed	
☐	☒	The exact sample size (*n*) for each experimental group/condition, given as a discrete number and unit of measurement
☐	☒	A statement on whether measurements were taken from distinct samples or whether the same sample was measured repeatedly
☐	☒	The statistical test(s) used AND whether they are one- or two-sided *Only common tests should be described solely by name; describe more complex techniques in the Methods section.*
☐	☒	A description of all covariates tested
☐	☒	A description of any assumptions or corrections, such as tests of normality and adjustment for multiple comparisons
☐	☒	A full description of the statistical parameters including central tendency (e.g. means) or other basic estimates (e.g. regression coefficient) AND variation (e.g. standard deviation) or associated estimates of uncertainty (e.g. confidence intervals)
☐	☒	For null hypothesis testing, the test statistic (e.g. *F*, *t*, *r*) with confidence intervals, effect sizes, degrees of freedom and *P* value noted *Give P values as exact values whenever suitable.*
☒	☐	For Bayesian analysis, information on the choice of priors and Markov chain Monte Carlo settings
☒	☐	For hierarchical and complex designs, identification of the appropriate level for tests and full reporting of outcomes
☒	☐	Estimates of effect sizes (e.g. Cohen's *d*, Pearson's *r*), indicating how they were calculated

Our web collection on statistics for biologists contains articles on many of the points above.

Software and code

Policy information about availability of computer code

Data collection	FACSDiva version 9.0; NextSeq500 (Illumina)
Data analysis	GraphPad Prism (version 8.4.0); R (version 4.1.1); Microsoft Excel (version 16.43); FlowJo (version 10.3); Columbus Image Data Storage and Analysis System; CellRanger (version 6.1.2); Python (version 3.8.8); GlycanAssure Data Acquisition Software (version 1.0) R packages used: corrplot (version 0.92); ggplot2 (version 3.3.5); gplots (version 3.1.1); factoextra (version 1.0.7); ggpubr (version 0.4.0); Seurat (version 4.0.0) Custom code to reproduce computational analyses available at: https://github.com/eirvine94/tb_fc_engineering_manuscript

For manuscripts utilizing custom algorithms or software that are central to the research but not yet described in published literature, software must be made available to editors and reviewers. We strongly encourage code deposition in a community repository (e.g. GitHub). See the Nature Portfolio guidelines for submitting code & software for further information.

Data

Policy information about [availability of data](#)

All manuscripts must include a [data availability statement](#). This statement should provide the following information, where applicable:

- Accession codes, unique identifiers, or web links for publicly available datasets
- A description of any restrictions on data availability
- For clinical datasets or third party data, please ensure that the statement adheres to our [policy](#)

> RNAseq data have been deposited in the Gene Expression Omnibus under accession number GSE271079. All other data and metadata associated with this study are available in the main text, Supplementary Information and/or at: https://fairdomhub.org/studies/1089.

Research involving human participants, their data, or biological material

Policy information about studies with [human participants or human data](#). See also policy information about [sex, gender (identity/presentation), and sexual orientation](#) and [race, ethnicity and racism](#).

Reporting on sex and gender	Investigators did not have access to information on sex and gender. The specimens used in this study were provided either coded or anonymized to protect the identity of the donors. For any coded specimens, the investigators did not have access to the key to the code and did not seek out the key. An agreement is in place between the investigators and the sample provider, ensuring that these identifiers will never be made known. As such, this study does not involve human subjects research.
Reporting on race, ethnicity, or other socially relevant groupings	Investigators did not have access to information on race, ethnicity, or other socially relevant groupings. The specimens were provided either coded or anonymized to protect the identity of the donors. For any coded specimens, the investigators did not have access to the key to the code and did not seek out the key. An agreement is in place between the investigators and the sample provider, ensuring that these identifiers will never be made known. As such, this study does not involve human subjects research.
Population characteristics	The samples used in this study were from the blood of healthy, human immunodeficiency virus-negative subjects. The specimens were provided anonymized or coded.
Recruitment	The samples used in this study are primary immune cells derived from human whole-blood and buffy coats. These specimens were obtained from healthy, human immunodeficiency virus (HIV)-negative subjects, who were recruited through a voluntary donation program conducted at Massachusetts General Hospital. Participants were informed about the study through informational sessions and written materials, and those interested underwent screening for eligibility. Eligibility criteria included the absence of clinical signs of illness and negative test results for active HIV, hepatitis C virus (HCV), and hepatitis B virus (HBV) infections. No demographic characteristics, such as age, gender, or ethnicity, were used as selection criteria to ensure a diverse and representative sample. The specimens were provided either coded or anonymized to protect the identity of the donors. For any coded specimens, the investigator did not have access to the key to the code and did not seek out the key. An agreement is in place between the investigator and the sample provider, ensuring that these identifiers will never be made known. Additionally, the samples were provided by individuals who did not have any role in the research study.
Ethics oversight	All donors provided written, informed consent. The study was approved by the institutional review board at Massachusetts General Hospital.

Note that full information on the approval of the study protocol must also be provided in the manuscript.

Field-specific reporting

Please select the one below that is the best fit for your research. If you are not sure, read the appropriate sections before making your selection.

☒ Life sciences   ☐ Behavioural & social sciences   ☐ Ecological, evolutionary & environmental sciences

For a reference copy of the document with all sections, see [nature.com/documents/nr-reporting-summary-flat.pdf](#)

Life sciences study design

All studies must disclose on these points even when the disclosure is negative.

Sample size	Sample sizes were determined was based on guidelines and findings from previously published studies using similar systems serology and Fc engineering approaches. Specifically, we reviewed other studies such as Gunn...Alter. Immunity 2021 (PMC8111768) and Irvine...Alter. Nature Immunology 2021 (PMC8642241), which employed similar experimental frameworks, taking into consideration the effect sizes, variability and statistical power reported. These studies provided a benchmark for selecting sample sizes that would ensure robust and reproducible results while maintaining ethical considerations regarding the use of biological samples.
Data exclusions	No data were excluded from the analyses.
Replication	Reported experiments were reproducible. Systems serology measurements were captured over 2 independent runs in technical duplicate;

Replication	replicates were minimally different. Mtb infection assays were performed in triplicate using cells from at least 2 healthy human donors. Single cell RNA-seq experiment was performed using cells from 3 healthy human donors.
Randomization	Randomization was not applied to this study because it did not involve research subjects or participants. The study was conducted using in vitro assays and controlled laboratory experiments with predefined conditions and parameters. The focus was on the functional consequences of antibody Fc engineering in the context of Mtb infection, where randomization is not typically a requirement. Instead, we ensured experimental rigor through replication, the use of appropriate controls, and standardized procedures to minimize bias and variability.
Blinding	Investigators were not blinded during the experiments herein because the nature of the experimental design required the investigators to be aware of the specific treatments and conditions being applied. This awareness was necessary for the accurate preparation, handling, and application of the antibodies, as well as for the precise monitoring of experimental variables. However, to mitigate potential bias, we employed standardized protocols, included appropriate controls, and conducted multiple replicates.

Reporting for specific materials, systems and methods

We require information from authors about some types of materials, experimental systems and methods used in many studies. Here, indicate whether each material, system or method listed is relevant to your study. If you are not sure if a list item applies to your research, read the appropriate section before selecting a response.

Materials & experimental systems

n/a	Involved in the study
☐	☒ Antibodies
☐	☒ Eukaryotic cell lines
☒	☐ Palaeontology and archaeology
☒	☐ Animals and other organisms
☒	☐ Clinical data
☒	☐ Dual use research of concern
☒	☐ Plants

Methods

n/a	Involved in the study
☒	☐ ChIP-seq
☐	☒ Flow cytometry
☒	☐ MRI-based neuroimaging

Antibodies

| Antibodies used | BioLegend:
anti-human CD66b-Pacific Blue \| clone G10F5 \| lot B256448\| cat 305112
anti-IFNγ \| clone B27 \| cat 506502

BD Biosciences:
PE-Cy7 anti-human CD56 \| clone B159 \| lot 0274120 \| cat 557747
APC-Cy7 anti-human CD16 \| clone 3G8 \| lot 9289979\| cat 557758
Alexa Fluor 700 anti-human CD3 \| clone UCHT1 \| lot 7145618\| cat 557943
PE anti-human MIP-1β \| clone D21-1351 \| lot 0065243 \| cat 550078
FITC anti-human IFNγ \| clone 25723.11 \| lot 0342682\| cat 340449
PE-Cy5 anti-human CD107a \| clone H4A3 (RUO) \| lot 0149826 \| cat 555802

BioXcell:
Human IgG1 isotype control \| clone N/A \| lot 659518A1 \| cat BE0297

MP Biomedicals:
FITC anti-guinea pig complement C3 \| lot 07927 \| cat 55385

ThermoFisher:
HRP anti-human kappa light chain \| cat A18853 \| lot 67-50-041519

Immune Technology:
Human IgG1 isotype control \| clone 37G12 \| lot 090327-AB005-01-18 \| cat IT-001-37G12

Invivogen:
Anti-IL-1β \| clone 4H5 \| cat mabg-hil1b-3 |
| Validation | All antibodies were used according to manufacturer's instructions and previously published methods. They were validated and titrated for specificity prior to use.

Antibody-dependent neutrophil phagocytosis, validation of CD66b antibody described in: PMID 27667685, PMID 29605231, PMID 30096313, PMID 30092199 PMID 30029854, and PMID 30629918.

Antibody-dependent NK cell activation, validation of antibodies described in: PMID 23468501, PMID 24648341, PMID 26745376, PMID 27667685, PMID 30096313, PMID 30092199, and PMID 30029854.

Antibody-dependent complement deposition, validation of antibodies described in: PMID 33852832 and PMID 31301278. |

Eukaryotic cell lines

Cell line source(s)	THP1 from ATCC cat TIB202; 293F from ThermoFisher cat R79007
Authentication	Cell lines commercially purchased. THP1 authentication was performed via STR Profiling service ATCC 135-XV. 293F cells were not authenticated.
Mycoplasma contamination	THP1 cell line was tested and negative for mycoplasma via ATCC Univ Mycoplasma kit 30-1012K. 293F cells were not tested for mycoplasma contamination.
Commonly misidentified lines (See ICLAC register)	No commonly misidentified cell lines were used.

Plants

Seed stocks	*Report on the source of all seed stocks or other plant material used. If applicable, state the seed stock centre and catalogue number. If plant specimens were collected from the field, describe the collection location, date and sampling procedures.*
Novel plant genotypes	*Describe the methods by which all novel plant genotypes were produced. This includes those generated by transgenic approaches, gene editing, chemical/radiation-based mutagenesis and hybridization. For transgenic lines, describe the transformation method, the number of independent lines analyzed and the generation upon which experiments were performed. For gene-edited lines, describe the editor used, the endogenous sequence targeted for editing, the targeting guide RNA sequence (if applicable) and how the editor was applied.*
Authentication	*Describe any authentication procedures for each seed stock used or novel genotype generated. Describe any experiments used to assess the effect of a mutation and, where applicable, how potential secondary effects (e.g. second site T-DNA insertions, mosiacism, off-target gene editing) were examined.*

Flow Cytometry

Plots

Confirm that:

☒ The axis labels state the marker and fluorochrome used (e.g. CD4-FITC).

☒ The axis scales are clearly visible. Include numbers along axes only for bottom left plot of group (a 'group' is an analysis of identical markers).

☒ All plots are contour plots with outliers or pseudocolor plots.

☒ A numerical value for number of cells or percentage (with statistics) is provided.

Methodology

Sample preparation	Fresh peripheral blood was collected from healthy donors in acid citrate dextrose (ACD) anti-coagulant tubes.
Instrument	BD LSRII
Software	FACSDiva (version 9.0) and FlowJo (version 10.3)
Cell population abundance	Cell sorting not performed.
Gating strategy	The flow cytometry gating strategy employed in this study began with initial gating on forward scatter (FSC) and side scatter (SSC) to identify single cells and exclude doublets. Specifically, an FSC-A versus FSC-H gate was used to select single cells, followed by an FSC-A versus SSC-A gate to exclude debris and dead cells, thereby focusing on the main population of viable cells. Negative controls were used to establish baseline autofluorescence and non-specific binding, setting thresholds for positive staining. Experimental samples were then gated using these thresholds to accurately define positive and negative populations. Marker-specific gating was applied to identify relevant cell populations. For instance, neutrophils were identified by gating on CD66b (PacBlue-A) following the selection of single, viable cells. Similarly, NK cells were gated using CD56 (PE-Cy7-A) and CD16 (APC-Cy7-A). Fluorescence Minus One (FMO) controls were utilized to set precise gates for positive and negative populations, accounting for background fluorescence. Sequential gating was then performed to further refine specific populations, such as CD107a, IFNγ, and MIP1b for functional assays. All gates were consistently applied across samples using FlowJo software to ensure reproducibility and accuracy. This comprehensive gating strategy enabled precise identification and quantification of cell populations, minimizing background noise and non-specific signals. See Extended Data Figure 7 for exact gating strategy.

☒ Tick this box to confirm that a figure exemplifying the gating strategy is provided in the Supplementary Information.